



# An animal model for mitochondrial tyrosyl-tRNA synthetase deficiency reveals links between oxidative phosphorylation and retinal function

Received for publication, September 9, 2020, and in revised form, February 9, 2021. Published, Papers in Press, February 19, 2021.

<https://doi.org/10.1016/j.jbc.2021.100437>

Xiaofen Jin<sup>1,2,3,†</sup>, Zengming Zhang<sup>3,†</sup>, Zhipeng Nie<sup>3</sup>, Chenghui Wang<sup>3</sup>, Feilong Meng<sup>2,3</sup>, Qiuzi Yi<sup>3</sup>, Mengquan Chen<sup>4</sup>, Jiji Sun<sup>3</sup>, Jian Zou<sup>5</sup>, Pingping Jiang<sup>2,3,6,\*</sup>, and Min-Xin Guan<sup>1,2,3,6,7,\*</sup>

From the <sup>1</sup>Key Laboratory of Reproductive Genetics, Ministry of Education of PRC, The Woman's Hospital, Zhejiang University School of Medicine, Hangzhou, Zhejiang, China; <sup>2</sup>Division of Medical Genetics and Genomics, The Children's Hospital, Zhejiang University School of Medicine, and National Clinic Research Center for Child Health, Hangzhou, Zhejiang, China; <sup>3</sup>Institute of Genetics, Zhejiang University School of Medicine, Hangzhou, Zhejiang, China; <sup>4</sup>Department of Lab Medicine, Wenzhou Hospital of Traditional Chinese Medicine, Wenzhou, Zhejiang, China; <sup>5</sup>Institute of Translational Medicine, Zhejiang University School of Medicine, Hangzhou, Zhejiang, China; <sup>6</sup>Zhejiang Provincial Key Laboratory of Genetic & Developmental Disorders, Zhejiang University, Hangzhou, Zhejiang, China; <sup>7</sup>Division of Mitochondrial Biomedicine, Joint Institute of Genetics and Genome Medicine between Zhejiang University and University of Toronto, Hangzhou, Zhejiang, China

Edited by Karin Musier-Forsyth

Mitochondria maintain a distinct pool of ribosomal machinery, including tRNAs and tRNAs activating enzymes, such as mitochondrial tyrosyl-tRNA synthetase (YARS2). Mutations in YARS2, which typically lead to the impairment of mitochondrial protein synthesis, have been linked to an array of human diseases including optic neuropathy. However, the lack of YARS2 mutation animal model makes us difficult to elucidate the pathophysiology underlying YARS2 deficiency. To explore this system, we generated YARS2 knockout (KO) HeLa cells and zebrafish using CRISPR/Cas9 technology. We observed the aberrant tRNA<sup>Tyr</sup> aminoacylation overall and reductions in the levels in mitochondrion- and nucleus-encoding subunits of oxidative phosphorylation system (OXPHOS), which were especially pronounced effects in the subunits of complex I and complex IV. These deficiencies manifested the decreased levels of intact supercomplexes overall. Immunoprecipitation assays showed that YARS2 bound to specific subunits of complex I and complex IV, suggesting the post-translational stabilization of OXPHOS. Furthermore, YARS2 ablation caused defects in the stability and activities of OXPHOS complexes. These biochemical defects could be rescued by the overexpression of YARS2 cDNA in the YARS2<sup>KO</sup> cells. In zebrafish, the *yars2*<sup>KO</sup> larva conferred deficient COX activities in the retina, abnormal mitochondrial morphology, and numbers in the photoreceptor and retinal ganglion cells. The zebrafish further exhibited the retinal defects affecting both rods and cones. Vision defects in *yars2*<sup>KO</sup> zebrafish recapitulated the clinical phenotypes in the optic neuropathy patients carrying the YARS2 mutations. Our findings highlighted the critical role of YARS2 in the stability and activity of OXPHOS and its pathological consequence in vision impairments.

Defects in mitochondrial protein synthesis are associated with a wide spectrum of human diseases, with a diversity of etiologies, ages of onset, involved organ systems and clinical presentations (1–3). Mitochondrial translation deficiencies resulted from defects in two rRNAs or 22 tRNAs, encoded by mitochondrial DNA (mtDNA), or alterations in the components of mitochondrial translation machinery (ribosomal proteins, ribosomal assembly proteins, aminoacyl-tRNA synthetases, tRNA-modifying enzymes, tRNA methylating enzymes, initiation, elongation, and termination factors), encoded by nuclear genes (3–9). In particular, all 19 mitochondrial aminoacyl-tRNA synthetases (mt-aaRSs) were synthesized in the cytosol and subsequently imported into mitochondria. These mt-aaRSs are a group of enzymes that catalyze a two-step reaction where they first activate the cognate amino acid with ATP to form an aminoacyl-adenylate, then subsequently transfer the aminoacyl group of the aminoacyl-adenylate to the bound tRNA for protein synthesis (8–10). In addition to their central roles in the translation, these aminoacyl-tRNA synthetases may have other functions, as in the case of cytoplasmic aminoacyl-tRNA synthetases (11–13). Defects in nuclear genes encoding mt-aaRSs have emerged as an important cause of mitochondrial disorders linked to diverse clinical presentations, usually with an early onset and transmitted as autosomal recessive traits (8–10, 14–16). Remarkably, the pathologies linked to defects in mt-aaRSs display a marked bias for the central nervous system, including the leukodystrophy, encephalopathy, Perrault syndrome, sensorineural deafness, and visual impairment (17–23). However, the pathophysiology of these disease-linked mt-aaRS mutations, especially the pleiotropic and tissue-specific effects, remains poorly understood.

Mutations of YARS2 gene encoding mitochondrial tyrosyl-tRNA synthetase were responsible for the myopathy, lactic acidosis, and sideroblastic anemia (MLASA) with

<sup>†</sup> The first two authors have equally contributed to this work.

\* For correspondence: Min-Xin Guan, [gminxin88@zju.edu.cn](mailto:gminxin88@zju.edu.cn), Pingping Jiang, [ppjiang@zju.edu.cn](mailto:ppjiang@zju.edu.cn).

## Critical roles of mitochondrial tyrosyl-tRNA synthetase

mitochondrial respiratory chain complex deficiencies (24–30). Recently, we demonstrated that the YARS2 p.Gly191Val mutation contributed to the phenotypic expression of Leber’s hereditary optic neuropathy (LHON)-associated mtDNA mutations or deafness-associated tRNA<sup>Ser(UCN)</sup> 7511A > G mutation (31, 32). The primary defects in these YARS2 mutations were the deficient aminoacylation of tRNA<sup>Tyr</sup> (30–32). The aberrant tRNA<sup>Tyr</sup> metabolism impaired mitochondrial translation, especially for the synthesis of polypeptides with high content of tyrosine codon such as ND4, ND5, ND6, and CO2 in cell lines carrying YARS2 mutations (24, 29, 31, 32). Strikingly, cell lines carrying the YARS2 mutations exhibited marked reductions in the nucleus-encoding mitochondrial proteins: NDUFS3 and NDUFB8 [subunits of NADH:ubiquinone oxidoreductase (complex I)] and COX10 [subunit of cytochrome c oxidase (complex IV)] (24, 29, 32). These implied that YARS2 may play an important role in the biogenesis of oxidative phosphorylation (OXPHOS) system (1). To test this hypothesis, we used CRISPR/Cas9 genomic editing approach in HeLa cells to produce the targeted deletion in YARS2 gene. To further confirm the defects of YARS2 knockout (KO) (YARS2<sup>KO</sup>) in the HeLa cells, we transferred a plasmid carrying the full-length YARS2 cDNA into the YARS2<sup>KO</sup> HeLa cells. The YARS2<sup>KO</sup> cell lines were assessed for the effects of YARS2 mutations on the biogenesis of OXPHOS, by western blot analysis using the subunits of OXPHOS and

activity of respiratory chain complexes. To examine whether YARS2 interacts with the OXPHOS, we performed the immunoprecipitation assay using FLAG and HA antibodies in mitochondria of HeLa cell lines. To investigate whether defects in *yars2* caused the visual impairment *in vivo*, we investigated the *yars2* knockout zebrafish produced by genome editing using the CRISPR/Cas9 system.

## Results

### Generation of YARS2 knockout HeLa cell lines

To gain overall information on how the YARS2 deficiency affected the mitochondrial functions, we used CRISPR/Cas9 genomic editing approach to produce the targeted deletion in YARS2 gene in the HeLa cells. As a result, an allele, YARS2<sup>del14bp</sup>, was generated by introducing a 14 bp deletion in the exon 1 of YARS2 (homozygous cells were described as YARS2<sup>KO</sup> and wild type as WT). The 14 bp deletion resulted in a frameshift from codon 10, the introduction of a premature stop at codon 25 (p.Pro25\*), and truncated protein with 24 amino acids (Fig. 1A, Fig. S1). This allele was confirmed by Sanger sequencing, restriction fragment length polymorphism (RFLP) with digested with *Bst*NI (Fig. S1) and western blot analysis (Fig. 1B).

Defects in tRNA aminoacylation of tRNA<sup>Tyr</sup> were assessed by using electrophoresis in an acid polyacrylamide/urea gel system to separate uncharged tRNA species from the

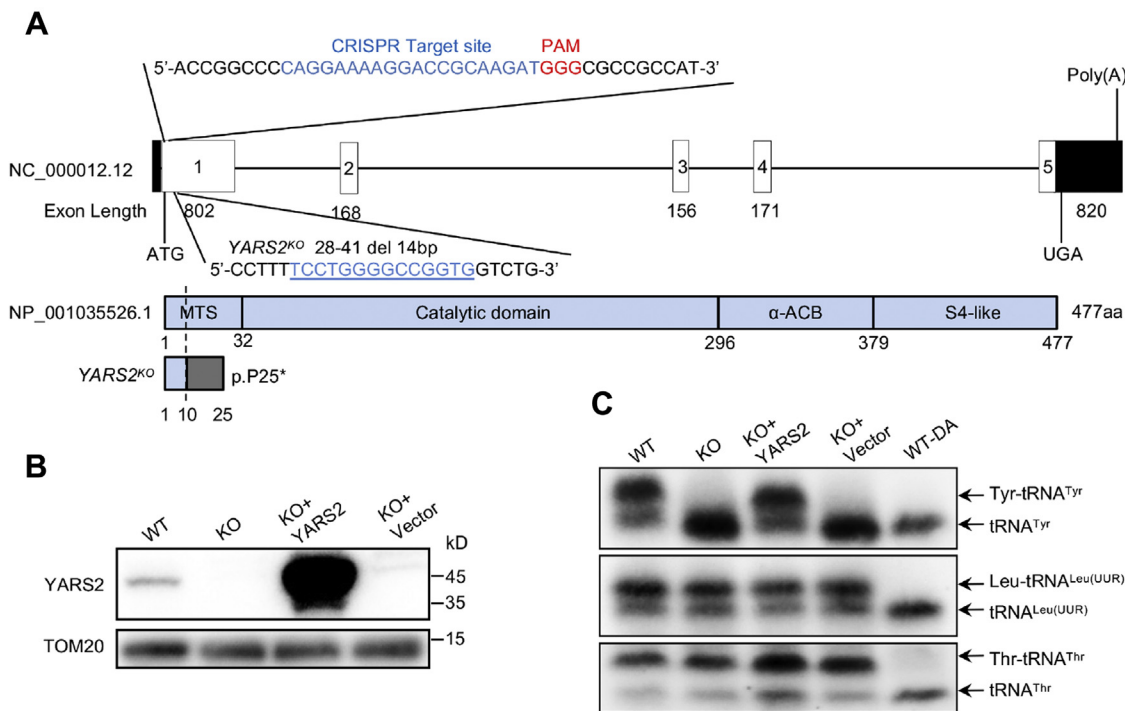


**Figure 1. Generation of YARS2 knockout HeLa cell lines using CRISPR/Cas9 system.** A, schematic representation of CRISPR/Cas9 target site at exon 1 as used in this study. An allele, YARS2<sup>del14bp</sup> was produced by a 14 bp delete in the exon 1 and a truncated nonfunctional protein with 24 amino acids. B, western blot analysis of YARS2 in various cells. Twenty micrograms of total cellular proteins of each cell line was electrophoresed through and hybridized with antibodies specific for YARS2 (1:1000 dilution) and with TOM20 (1:2000 dilution) as a loading control. WT, wild-type cells; KO, YARS2<sup>KO</sup>; KO+YARS2, exogenous YARS2 expression in YARS2<sup>KO</sup>; KO+vector, vector transfected in YARS2<sup>KO</sup>. Three independent experiments were performed. C, *in vivo* aminoacylation of mitochondrial tRNA assays. Ten micrograms of total cellular RNAs purified from various cell lines under acid conditions was electrophoresed through an acid (pH 5.2) 10% polyacrylamide-7 M urea gel, electroblotted, and hybridized with DIG-labeled oligonucleotide probe specific for the tRNA<sup>Tyr</sup>, tRNA<sup>Leu(UUR)</sup>, and tRNA<sup>Thr</sup>, respectively. Samples for WT cells were deacylated (DA) by heating for 10 min at 60 °C at pH 8.3, electrophoresed, and hybridized with DIG-labeled oligonucleotide probes as described above. Three independent experiments were performed.

corresponding charged tRNA, electroblotting and hybridizing with DIG-labeled probes specific for tRNA<sup>Tyr</sup>, tRNA<sup>Leu(UUR)</sup>, and tRNA<sup>Thr</sup>. As shown in Figure 1C, the slower migrating band (upper band) in WT cells represents the charged tRNA, and the faster migrating band (lower band) represents uncharged tRNA. However, only one lower band in the tRNA<sup>Tyr</sup> but two bands of tRNA<sup>Leu(UUR)</sup> and tRNA<sup>Thr</sup> were detected in the YARS2<sup>KO</sup> cells, indicating that the ablation of YARS2 led to the complete loss of aminoacylation of tRNA<sup>Tyr</sup> but did not affect the aminoacylation of tRNA<sup>Leu(UUR)</sup> and tRNA<sup>Thr</sup>. To

further distinguish nonaminoacylated tRNA from aminoacylated tRNA, samples of tRNAs were deacylated after heating for 10 min at 60 °C (pH 8.3) and then run in parallel. As shown in Figure 1C, the deacylated samples gave only one band (uncharged tRNA) in both mutant and control cell lines. To further confirm the ablation of YARS2 in HeLa cells, we transferred a plasmid carrying the full-length YARS2 cDNA into the YARS2<sup>KO</sup> cells. Indeed, the overexpression of YARS2 reversed the deficient aminoacylation of tRNA<sup>Tyr</sup> in the YARS2<sup>KO</sup> cells.

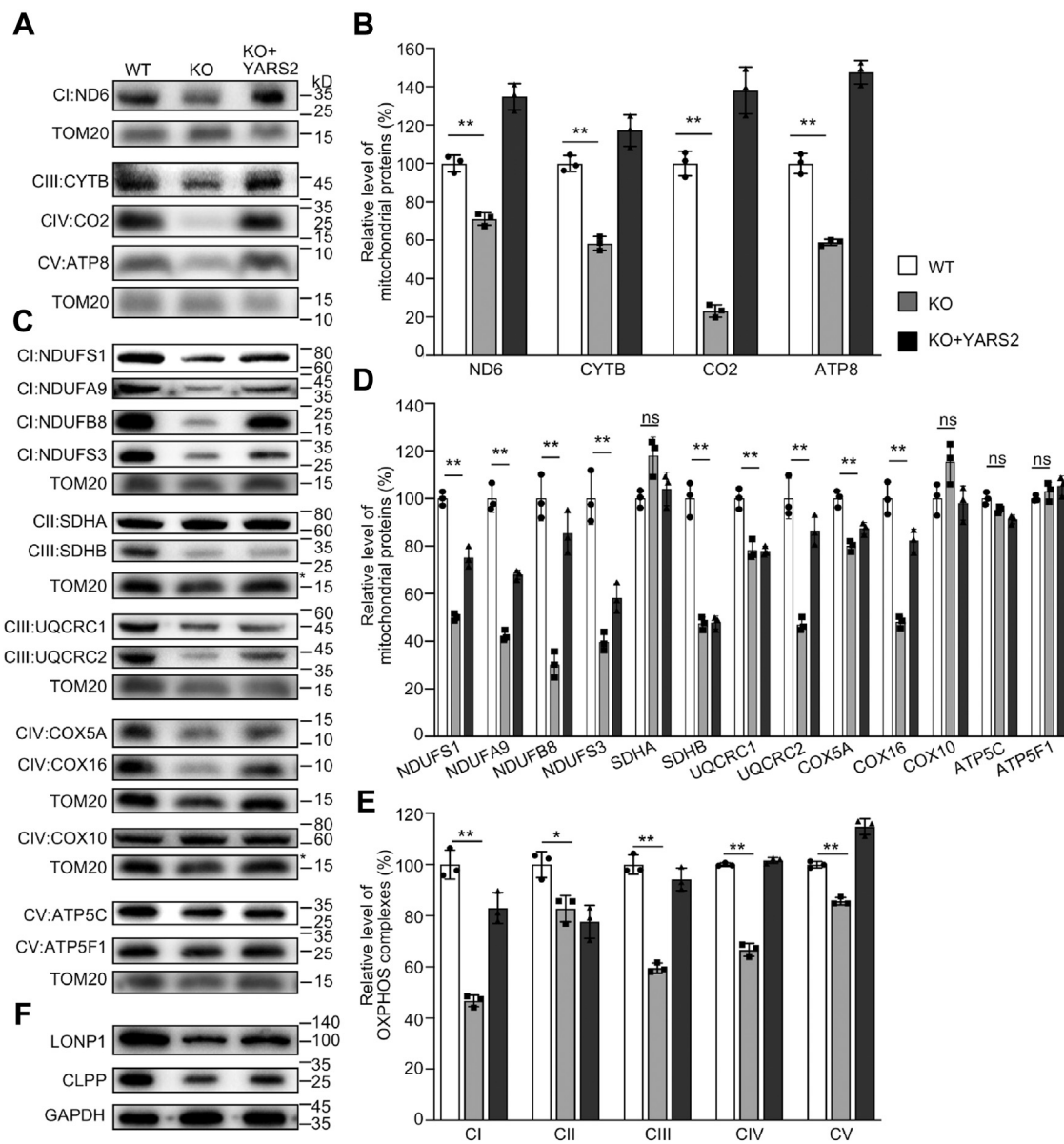


**Figure 2. Western blotting analysis of mitochondrial proteins.** A and C, twenty micrograms of total cellular proteins from various cell lines was electrophoresed through a denaturing polyacrylamide gel, electroblotted, and hybridized with antibodies for 17 subunits of OXPHOS (4 encoded by mtDNA and 13 encoded by nuclear genes), and TOM20 as a loading control, respectively. B and D, quantification of mitochondrial proteins: four mtDNA-encoding subunits (B) and 13 nucleus-encoding subunits (D). Average relative each polypeptide content per cell was normalized to the average content per cell of Tom20 in each cell line. The values for the latter are expressed as percentages of the average values for the WT HeLa cell line. The calculations were based on three independent determinations. The error bars indicate two standard deviations (SD) of the means. *p* indicates the significance, according to the *t*-test, of the differences between mutant and control cell lines. \**p* < 0.05; \*\**p* < 0.001; \*\*\**p* < 0.0001; ns, not significant. E, average levels of subunits from each complex of OXPHOS (5 of complexes I, 2 of II, 3 of III, 4 of IV, and 3 of V). The calculations were based on three independent determinations. Graph details and symbols are explained as above. F, western blot analysis of Clpp involved in mitochondrial ribosome assembly and LONP1 that is a nuclear-encoded mitochondrial protease.

## Critical roles of mitochondrial tyrosyl-tRNA synthetase

***YARS2*<sup>KO</sup> cells exhibited the reductions in the levels in the subunits of OXPHOS, reversible by overexpression of *YARS2***

To assess the effect of *YARS2* mutation on the OXPHOS biogenesis, we carried out the western blotting analysis to examine the levels in 17 subunits of OXPHOS complexes in *YARS2*<sup>KO</sup> and WT cells using TOM20 as a loading control. These subunits included four mtDNA-encoding polypeptides (ND6, CYTB, CO2, and ATP8), 13 nucleus-encoding proteins: NDUFS1, NDUFS3, NDUFA9, and NDUFB8 (subunits of complex I), SDHA and SDHB [subunits of succinate dehydrogenase (complex II)], UQCRC1 and UQCRC2 [subunits of ubiquinol-cytochrome c reductase (complex III)], COX5A, COX10, and COX16 (subunits of complex IV), and ATP5C and ATP5F1 [subunits of H<sup>+</sup>-ATPase (complex V)] (1). As shown in Figure 2, A and C, the various decreases in the levels of 13 mitochondrial proteins (but not of SDHA, COX10, ATP5C, and ATP5F1) were observed in the *YARS2*<sup>KO</sup> cells, as compared with the WT cells. As shown in Figure 2B, the levels of ND6, CYTB, CO2, and ATP8 in the *YARS2*<sup>KO</sup> cells were 71%, 58%, 23%, and 59%, with an average of 53%, relative to the mean values measured in the WT cells. As shown in the

Figure 2D, the levels of NDUFS1, NDUFS3, NDUFA9, NDUFB8, SDHA, SDHB, UQCRC1, UQCRC2, COX5A, COX10, COX16, ATP5C, and ATP5F1 in *YARS2*<sup>KO</sup> cells were 50%, 40%, 42%, 30%, 118%, 48%, 78%, 47%, 80%, 115%, 48%, 95%, and 103%, relative to the mean values measured in the WT cells, respectively. Notably, the average levels in the subunits of complexes I, II, III, IV, and V in the *YARS2*<sup>KO</sup> cells were 47%, 82%, 60%, 66%, and 85% of average values measured in the WT HeLa cells, respectively (Fig. 2E). However, the overexpression of *YARS2* elevated the levels of these subunits.

To test whether the *YARS2* deficiency affected the mitochondrial proteostasis, we measured the levels of Clpp involved in mitochondrial ribosome assembly (33) and LONP1 that is a nuclear-encoded mitochondrial protease crucial for organelle homeostasis (34) in the *YARS2*<sup>KO</sup> and WT cells. As shown in Figure 2F, the levels of Clpp and LONP1 in the *YARS2*<sup>KO</sup> cells were 63% and 64% of those in the WT cells, respectively. These indicated that *YARS2* deletion impaired mitochondrial proteostasis.

To further examine the effect of *YARS2* mutation on the OXPHOS, we undertook the western blotting analysis to

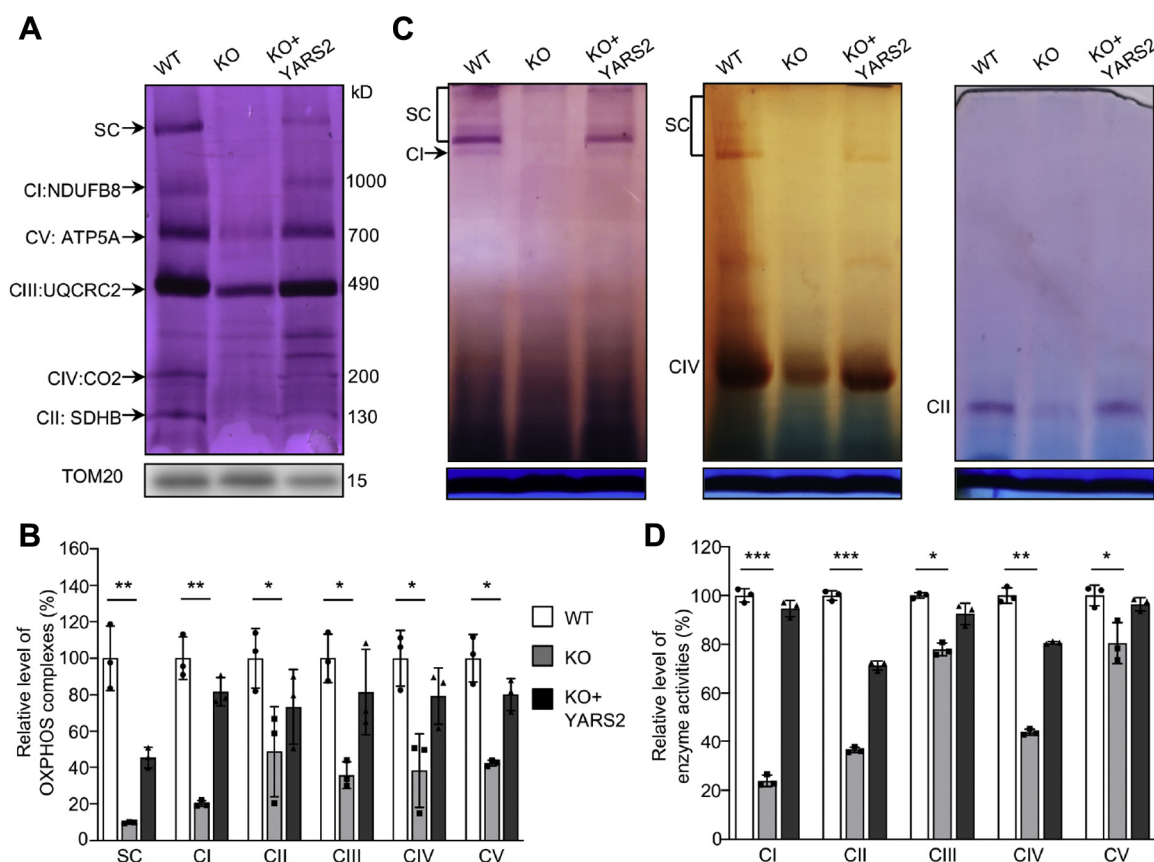


**Figure 3. Analysis of stability and activity of OXPHOS complexes.** A, assembly and stability of OXPHOS complexes. Mitochondria extracted from various cell lines were solubilized with n-dodecyl- $\beta$ -D-maltoside, electroblotted, and hybridized with antibody cocktail specific for subunits of five OXPHOS complexes and with TOM20 as a loading control. B, quantification of the levels of complexes I, II, III, IV, V and supercomplexes (SC) in mutant and wild-type cell lines. The calculations were based on three independent determinations. C, in-gel activity of respiratory chain complexes I, II, and IV. A total of 20  $\mu$ g of mitochondrial proteins (8 g/g digitonin/protein ratio) from various cell lines was used for BN-PAGE, and the activities of complexes were measured in the presence of specific substrates (NADH and NTB for complex I, sodium succinate, phenazine methosulfate, and NTB for complex II, DAB and cytochrome c for complex IV). Coomassie staining was used as a loading control. D, enzymatic activities of respiratory chain complexes. The activities of respiratory complexes were investigated by enzymatic assay on complexes I, II, III, IV, and V in mitochondria isolated from various cell lines. The calculations were based on three independent experiments. Graph details and symbols are explained in the legend to Figure 2.

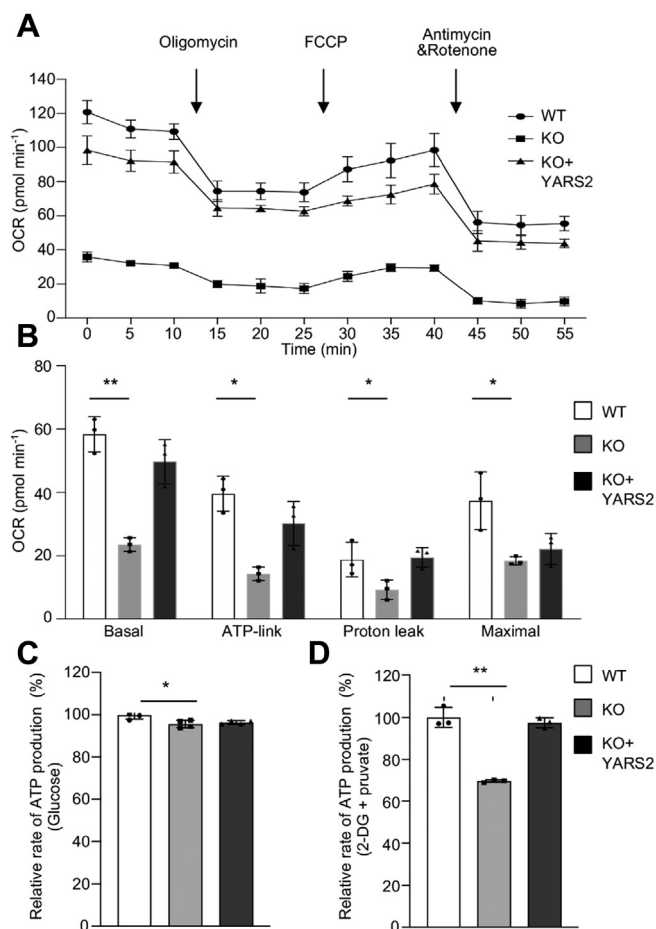


**Figure 4. Deficient oxidative phosphorylation.** *A*, an analysis of O<sub>2</sub> consumption in the various cell lines using different inhibitors. The rates of O<sub>2</sub> (OCR) were first measured on  $2 \times 10^4$  cells of each cell line under basal condition and then sequentially added to oligomycin (1.5 mM), carbonyl cyanide p-(trifluoromethoxy) phenylhydrazone (FCCP) (0.5 mM), rotenone (1.0 mM), and antimycin A (1.0 mM) at indicated times to determine different parameters of mitochondrial functions. *B*, graphs presented the basal OCR, ATP-linked OCR, proton leak OCR, and maximal OCR in cell lines. Basal OCR was determined as OCR before oligomycin minus OCR after rotenone/antimycin A. ATP-linked OCR was determined as OCR before oligomycin minus OCR after oligomycin. Proton leak was determined as Basal OCR minus ATP-linked OCR. Maximal was determined as the OCR after FCCP minus nonmitochondrial OCR. *C* and *D*, measurement of whole-cell and mitochondrial ATP levels using bioluminescence assay. Cells were incubated with 10 mM glucose or 5 mM 2-deoxy-d-glucose plus 5 mM pyruvate to determine ATP generation under mitochondrial ATP synthesis. Average rates of ATP level per cell line and are shown: (*C*) ATP levels in total cells. *D*, ATP levels in mitochondria. Three independent experiments were made for each cell line. Graph details and symbols are explained in the legend to Figure 2.

determine the levels in 15 subunits of OXPHOS complexes using lymphoblastoid cell line (I-1) bearing homozygous *YARS2* p.191Gly>Val mutation and control cell line (A61) lacking the mutation (32). These subunits included four mtDNA-encoding polypeptides (ND6, CYTB, CO2, and ATP8), 13 nucleus encoding proteins: NDUFS1, NDUFS3, NDUFB8, NDUFA9, SDHA, SDHB, UQCRC1, UQCRC2, COX5A, COX16, and ATP5F1. As shown in Fig. S2, A and C, the various decreases in the levels of 11 mitochondrial proteins (but not of NDUFB8, SDHA, COX16, and ATP5F1) were observed in the mutant cell line carrying the p.191Gly>Val

mutation, as compared with those in control line. As shown in Fig. S2B, the levels of ND6, CYTB, CO2, and ATP8 in the mutant cell line were 75%, 84%, 72%, and 89%, with an average of 80%, relative to the mean values measured in the control line. As shown in the Fig. S2D, the levels of NDUFS1, NDUFS3, NDUFB8, NDUFA9, SDHA, SDHB, UQCRC1, UQCRC2, COX5A, COX16, and ATP5F1 in the mutant cell line were 72%, 66%, 106%, 84%, 106%, 54%, 98%, 87%, 126%, 78%, and 131%, relative to the mean values measured in the control line, respectively. Notably, the average levels in the subunits of complexes I, II, III, IV, and V in the mutant cell line were 82%, 80%, 90%, 92%, and 110% of average values measured in the control line, respectively (Fig. S2E).

#### Deletion of *YARS2* altered the stability and activity of OXPHOS complexes

We analyzed the consequence of *YARS2* deletion on the oxidative phosphorylation machinery. Mitochondrial membrane proteins isolated from *YARS2*<sup>KO</sup> and WT cell lines were separated by BN-PAGE, electroblotting, and hybridizing with human OXPHOS antibody cocktail consisting of NDUFB8, ATP5A, UQCRC2, CO2, and SDHB. As illustrated in Figure 3A, the *YARS2*<sup>KO</sup> cells exhibited the instability of intact supercomplexes, complexes I, II, III, IV, and V. As shown in Figure 3B, the levels of supercomplexes, complexes I, II, III, IV, and V in the *YARS2*<sup>KO</sup> cells were 9.8%, 20.2%, 48.7%, 35.7%, 38.4%, and 42.3% of those average values in WT cells, respectively. Furthermore, we carried out the in-gel activity assays to verify the *YARS2* deletion-induced alterations in complexes I, II, and IV (35, 36). As shown in Figure 3C, the in-gel activities of complexes I, II, and IV were drastically decreased in the *YARS2*<sup>KO</sup> cells, as compared with the WT cells. We further measured the activities of OXPHOS complexes by the use of isolating mitochondria from mutant and control cell lines (36–38). The activity of complex I (NADH ubiquinone oxidoreductase) was determined through the oxidation of NADH with ubiquinone as the electron acceptor. The activity of complex II (succinate ubiquinone oxidoreductase) was examined the activity of complex II through the artificial electron acceptor DCPIP. The activity of complex III (ubiquinone cytochrome c oxidoreductase) was assessed through the reduction of cytochrome c (III) by using D-ubiquinol-2 as the electron donor. The activity of complex IV (cytochrome c oxidase) was monitored through the oxidation of cytochrome c (II). The activity of complex V (F1-ATP synthase) was explored through the NADH oxidation *via* conversion of phosphoenolpyruvate to lactate by two step reaction. As shown in Figure 3D, the average activities of complexes I, II, III, IV, and V in *YARS2*<sup>KO</sup> cells were 24%, 37%, 78%, 44%, and 80% of the mean value measured in WT cells, respectively. However, the overexpression of *YARS2* cDNAs in the *YARS2*<sup>KO</sup> cells restored the defects in the activities of these complexes.

#### Deficient oxidative phosphorylation

Oxygen consumption rate (OCR) is an indicator of mitochondrial respiration (39). Using the Seahorse Bioscience XF-96 Extracellular Flux Analyzer, we measured the OCRs of

## Critical roles of mitochondrial tyrosyl-tRNA synthetase

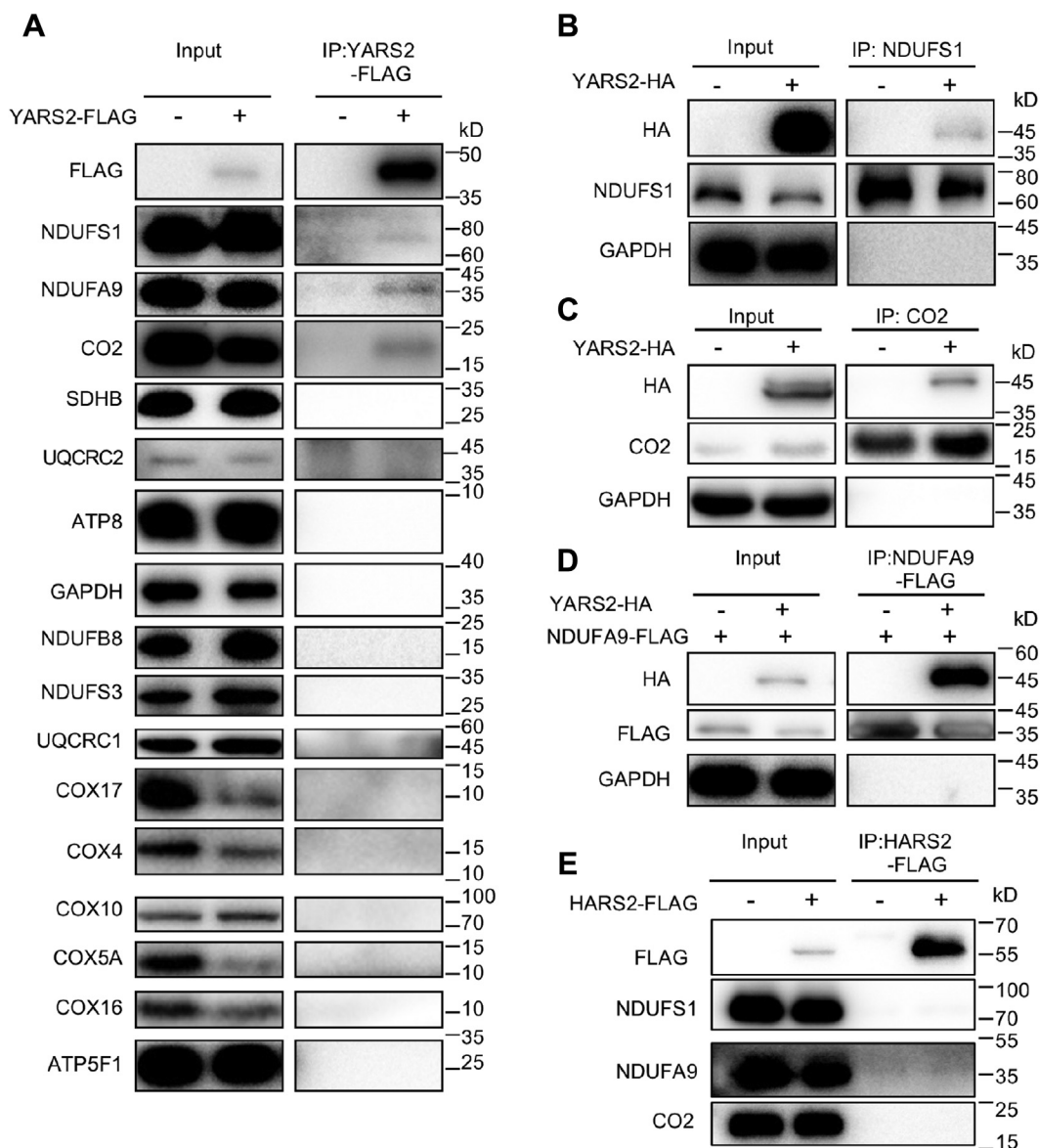


**Figure 5. Immunoprecipitation analysis of YARS2 with subunits of OXPHOS complexes.** A, co-immunoprecipitation of YARS2-FLAG and subunits of OXPHOS. HeLa cells transiently expressing with or without YARS2-FLAG were solubilized with a lysis buffer and lysate proteins were immunoprecipitated with immunocapture buffer (left) (input) and FLAG-antibody (right) (IP), respectively. Immunoprecipitates were analyzed by SDS-PAGE and western blotting using anti-FLAG, anti-subunits of OXPHOS (NDUFS1, NDUFS3, NDUFA9 and NDUFB8 for complex I, SDHB for complex II, UQCRC1 and UQCRC2 for complex III, CO2, COX4, COX5A, COX10, COX16, and COX17 for complex IV, ATP8 and ATP5F1 for complex V) and GAPDH antibodies, respectively. B and C, co-immunoprecipitation of YARS2-HA and NDUFS1, CO2 using anti-HA, anti-NDUFS1, CO2, and GAPDH antibodies, respectively. D, co-immunoprecipitation of YARS2-HA and NDUFA9-FLAG using anti-HA, anti-FLAG, and GAPDH antibodies, respectively. E, co-immunoprecipitation of HARS2-FLAG and NDUFS1, NDUFA9, CO2 in lysates of HeLa cells transfected with plasmids containing HARS2 using anti-FLAG, anti-NDUFS1, NDUFA9, and CO2 antibodies respectively.

various cell lines, including basal respiration,  $O_2$  consumption attributing to ATP production, proton leak, maximum respiratory rate, reserve capacity, and nonmitochondrial respiration (39, 40). As shown in Figure 4A, the average basal OCRs in the  $YARS2^{KO}$  cells were 40% ( $p < 0.001$ ) of the mean values measured in WT cells. To further investigate which of the enzyme complexes of the respiratory chain was affected in the  $YARS2^{KO}$  cells, OCR was monitored after the sequential addition of oligomycin (to inhibit the ATP synthase), FCCP (to uncouple the mitochondrial inner membrane and allow for maximum electron flux through the ETC), antimycin A (to

inhibit complex III), and rotenone (to inhibit complex I). As shown in Figure 4B, the ATP linked OCR, proton leak OCR, and maximal OCR in  $YARS2^{KO}$  cells were 36% ( $p < 0.01$ ), 50% ( $p < 0.05$ ), and 49% ( $p < 0.05$ ) relative to the mean values measured in the WT cells, respectively. As expected, the overexpression of YARS2 cDNAs in the  $YARS2^{KO}$  cells rescued the respiratory deficiency.

We then used the luciferin/luciferase assay to examine the capacity of oxidative phosphorylation in mutant and wild-type cell lines. Populations of cells were incubated in the media in the presence of glucose and 2-deoxy-D-glucose with pyruvate

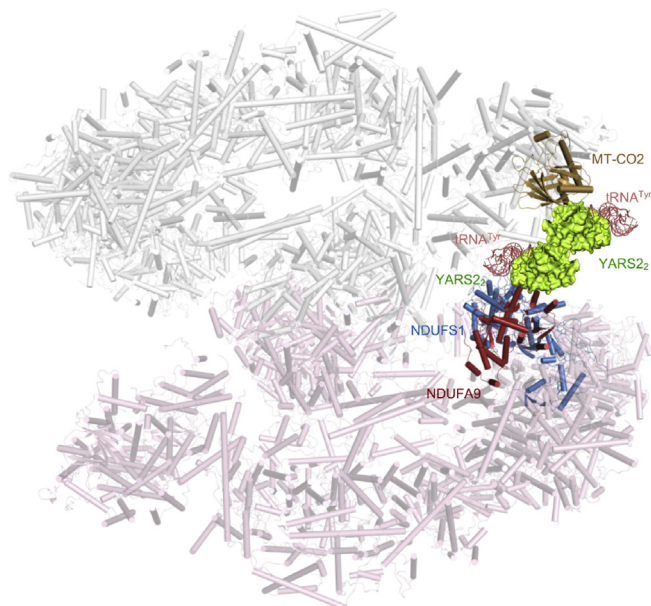


**Figure 6. The proposed model of YARS2 interacting with the OXPHOS supercomplex.** The partial OXPHOS supercomplex was derived from (MCI<sub>2</sub>III<sub>2</sub>IV<sub>2</sub>, PDB: 5XTI) (41). The structure of *Thermus thermophilus* tryrosyl-tRNA synthetase and tRNA<sup>Tyr</sup> complex (PDB ID: 1H3E) was used as an original templet for construction of the model of human YARS2-tRNA<sup>Tyr</sup> complex. The structure of YARS2 was extracted from the crystal structures of human mitochondrial tyrosyl-tRNA synthetase (PDB ID: 2PID) (42). The model of human YARS2-tRNA<sup>Tyr</sup> complex was generated using PyMOL molecular visualization system (PyMOL Molecular Graphics System, Version 2.3.3, Schrödinger, LLC). A model of YARS2 interacting with the OXPHOS supercomplex was proposed as the YARS2 homodimer-tRNA<sup>Tyr</sup> complex interacts with CO2 of CIV, NDUFS1 and NDUF9 of membrane arm of CI in the megacomplexes I<sub>2</sub>III<sub>2</sub>IV<sub>2</sub>, respectively.

(40). As shown in Figure 4C, the level of total ATP production in *YARS2*<sup>KO</sup> cells, with the presence of glucose, was comparable with those measured in WT cells. In contrast, the level of mitochondrial ATP production in *YARS2*<sup>KO</sup> cells, with the presence of 2-deoxy-D-glucose and pyruvate to inhibit the glycolysis, was 70% relative to the mean value measured in WT cells (Fig. 4D).

#### **YARS2 may interact with NDUFS1, NDUF9 of complex I, and CO2 of complex IV**

To test whether YARS2 interacted with the OXPHOS complex, we performed the immunoprecipitation assay using FLAG antibodies in mitochondria of HeLa cell lines overexpressed with human FLAG-tagged YARS2. As shown in Figure 5A, the YARS2-FLAG antibody reciprocally immunoprecipitated to NDUFS1, NDUF9 of CI subunits, and CO2 of CIV subunit, but did not bind to NDUF8 and NDUFS3 of CI subunits, SDHB of CII subunit, UQCRC1 and UQCRC2 of CIII subunits, COX4, COX5A, COX10, COX16, and COX17 of CIV subunits, ATP8 and ATP5F of CV subunits, respectively. These data indicated the potential interactions of YARS2 with complex I and complex IV by binding to NDUFS1, NDUF9, and CO2, respectively. These interactions of YARS2 with these three subunits were verified by the fact that antibodies against NDUFS1, FLAG-NDUF9, and CO2

co-immunoprecipitated with the HA-tagged YARS2. However, the CO-IP signal of NDUFS1 with YARS2 was much weaker than those of CO2, suggesting that the interaction of YARS2 with NDUFS1 may be very weak and unstable. Furthermore, Flag-tagged mitochondrial histidyl-tRNA synthetase (HARS2) was overexpressed in HeLa cells for immunoprecipitation as a negative control. As shown Figure 5E, FLAG-HARS2 did not co-immunoprecipitate NDUFS1, NDUF9, or CO2, indicating no interaction of HARS2 to these subunits. Moreover, immunofluorescence staining experiments showed that a carboxy terminus FLAG or HA-tagged YARS2 displayed the overlap with CO2, NDUFS1, NDUF9, and NDUFS3, respectively, with a significant correlation (Pearson's coefficient of 0.59, 0.71, 0.73, and 0.45, respectively) (Fig. S3). These data suggested the potential direct interaction of YARS2 with NDUFS1, NDUF9, and CO2, respectively.

The overall structure of supercomplexes (MCI<sub>2</sub>III<sub>2</sub>IV<sub>2</sub>, PDB: 5XTI) showed that the NDUFS1, interacting with NDUF9, were the components of matrix arm of CI (41). As shown in Figure 6, there was a pocket formed by CO2 of CIV together with NDUFS1 and NDUF9 of membrane arm of CI in the megacomplexes I<sub>2</sub>III<sub>2</sub>IV<sub>2</sub>. This pocket may provide an interspace for the interactions of YARS2 with complex I and complex IV. As YARS2 functioned usually as a homodimer (PDB: 2PID) (42), we proposed that the YARS2 homodimer with tRNA<sup>Tyr</sup> complex resided at the pocket as a component of supercomplexes by interacting with CI and CIV. Therefore, YARS2 may play a critical role in the formation of the megacomplex in mitochondrial respiratory chain.

#### **Generation of *yars2* knockout zebrafish using CRISPR/Cas9 system**

To investigate the pathological impact of *yars2* deficiency *in vivo*, we used the CRISPR/Cas9 technology to produce zebrafish mutant lines as described elsewhere (43, 44). A single-guide RNA (sgRNA) targeting exon 1 of *yars2* was coinjected with Cas9 mRNA into wild-type one-cell stage embryos (Fig. S4). As a consequence, a 5 bp deletion at positions (c.117 T to c.121 G) in the exon 1 was produced (heterozygous and homozygous zebrafish were described as *yars2*<sup>+/-</sup>, *yars2*<sup>-/-</sup>, and wild type as *yars2*<sup>+/+</sup>). In fact, this deletion introduced a premature stop at codon 42 (p.L42\*) and subsequently propagated after the confirmation of the mutation by Sanger sequencing and western blot analysis (Fig. S4). The *yars2*<sup>-/-</sup> zebrafish were larval lethal before 10 dpf, while *yars2*<sup>+/-</sup> zebrafish were adult-viable. As shown in Figure 7, A and B, marked reductions of black-stained organ in the abdomen were observed in the *yars2*<sup>-/-</sup> larva at 5 dpf, as compared with those in the WT and *yars2*<sup>+/-</sup> larva. However, we did not see significant changes of the body lengths in *yars2*<sup>-/-</sup> and *yars2*<sup>+/-</sup> larval at 5 dpf (Fig. 7A, Fig. S5). As an assay of function, we also analyzed heart beat rates in 32 s at *yars2*<sup>-/-</sup>, *yars2*<sup>+/-</sup>, and wild-type larval at 5 dpf. As shown in Fig. S5B, there were no significant differences in the heart beat rates between *yars2*<sup>+/+</sup> and *yars2*<sup>-/-</sup> or *yars2*<sup>+/-</sup> larval.

## Critical roles of mitochondrial tyrosyl-tRNA synthetase

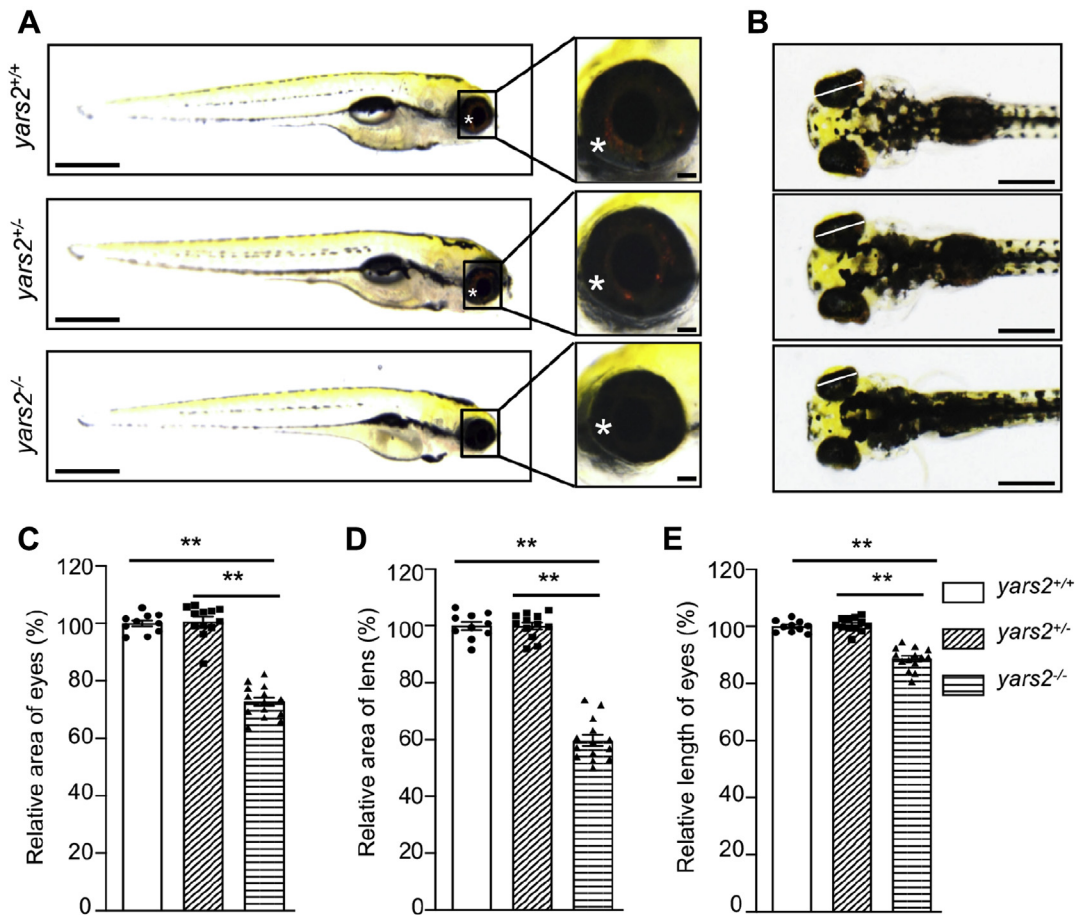


**Figure 7. Deletion of *yars2* caused the eye defects in zebrafish.** *A*, the lateral views of *yars2*<sup>-/-</sup>, *yars2*<sup>+/-</sup>, and *yars2*<sup>+/+</sup> zebrafish at 5 dpf, and the eye morphologies of zebrafish were illustrated under a Leica microscope with an objective magnification of 20x. Asterisk indicated the eye pigments. *B*, the dorsal views of the *yars2*<sup>+/+</sup>, *yars2*<sup>+/-</sup>, and *yars2*<sup>-/-</sup> zebrafish at 5 dpf. *C–E*, quantification of the area and length of eyes as well as area of lens of *yars2*<sup>+/+</sup> (*n* = 10), *yars2*<sup>+/-</sup> (*n* = 12), and *yars2*<sup>-/-</sup> (*n* = 14) zebrafish, as detailed elsewhere (47). The values for the mutants were expressed as percentages of the average values for the wild type. Graph details and symbols are explained in the legend to Figure 2.

### Loss of *yars2* caused the retinal defects in zebrafish at 5 dpf

Zebrafish is visually responsive by 72 h post fertilization and has functional retina at 5 dpf (45). The retina of zebrafish is composed of five layers [outer nuclear layer (ONL), outer plexiform layer (OPL), inner nuclear layer (INL), inner plexiform layer (IPL), and ganglion cell layer (GCL)] (46). As shown in Figure 7A, *yars2*<sup>-/-</sup> larvae at 5 dpf exhibited faint pigments, as compared with those in WT larvae. We then evaluated the sizes of eyes and lens in the zebrafish at 5 dpf (46). As shown in Figure 7, C, D and E, *yars2*<sup>-/-</sup> larvae revealed significant decreases in the average areas (72.8%) of eyes, average areas (59.7%) of lens, and average lengths (88.7%) of eyes, as compared with those in the *yars2*<sup>+/+</sup> larvae, respectively. However, there were no differences of those parameters between *yars2*<sup>+/-</sup> and *yars2*<sup>+/+</sup> larvae.

We then assessed whether the loss of *yars2* altered the thickness of layers in zebrafish retina using hematoxylin and eosin (H&E)-stained retinal sections from larvae at 5 dpf. As shown in Figure 8A, the ablation of *yars2* did not change the thickness in layers of pigmented epithelium (RPE), INL, IPL, and GCL, whereas the ONLs (containing the rod and cone granules: photoreceptor cells) in *yars2*<sup>-/-</sup>

larvae were reduced 20%, as compared with those in the *yars2*<sup>+/+</sup> larvae.

We further examined the morphology of cones and rods by immunolabeling with their specific markers, peanut agglutinin lectin (PNA-488) for cone and rhodopsin (prototypical G-protein-coupled receptor) for rods, respectively. As shown in Figure 8B, the outer segments of cones (staining with PNA-488) in the *yars2*<sup>-/-</sup> larvae were much shorter than those in the *yars2*<sup>+/+</sup> larvae (47). Moreover, the outer segments of rods (staining with rhodopsin) in the *yars2*<sup>-/-</sup> larvae were much less than those in *yars2*<sup>+/+</sup> larvae, indicating that the loss of *yars2* may affect the cone and rod developments (47). Furthermore, drastic changes of the layer below the rods were observed in the *yars2*<sup>-/-</sup> larval, as compared with those in the *yars2*<sup>+/+</sup> larval. However, there were no significant differences of morphology of cones and rods between *yars2*<sup>+/-</sup> and *yars2*<sup>+/+</sup> larvae. These data implied that the *yars2* deficiency led to the defects of retina, especially for photoreceptor degeneration.

### Mitochondrial defects in retina

Mitochondrial dysfunctions in retina were assessed by the enzyme histochemistry (EHC) staining for SDH and COX in

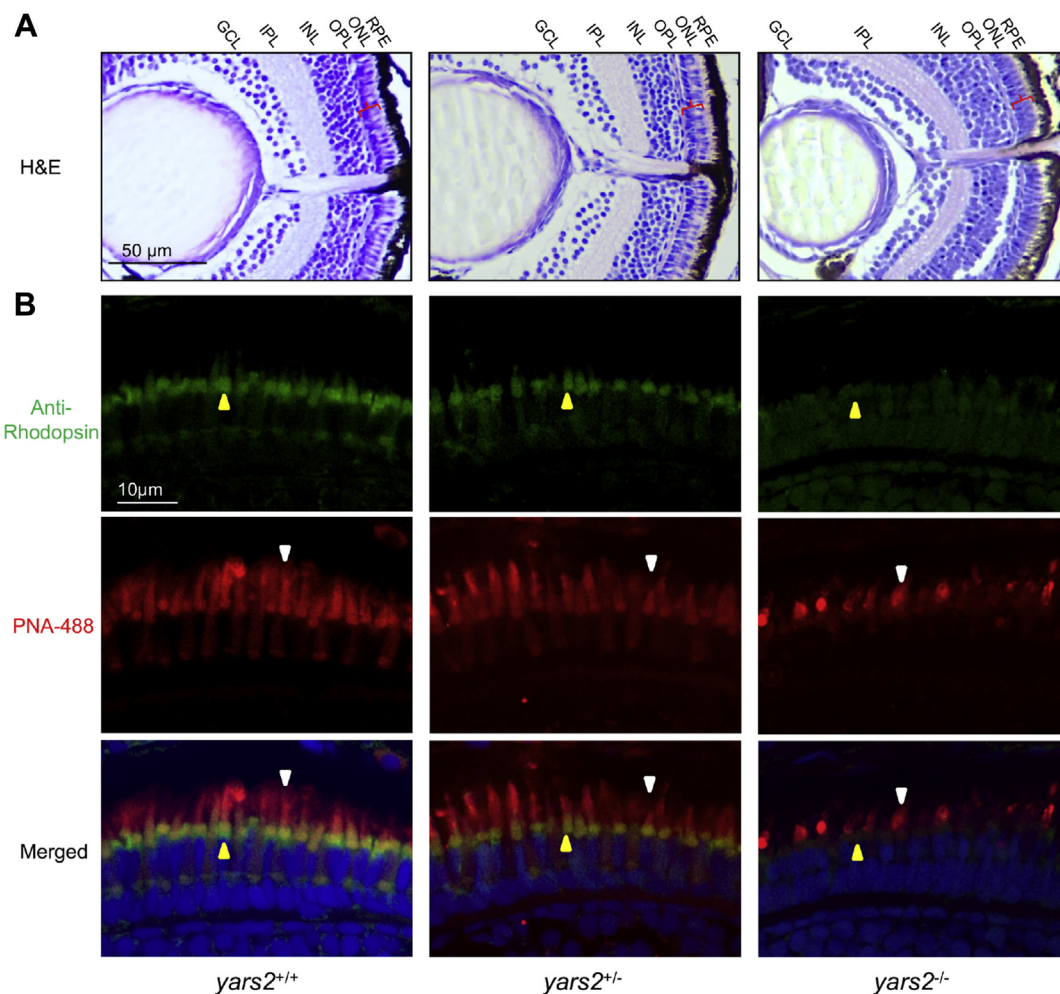


**Figure 8. Retina defects in zebrafish.** *A*, hematoxylin and eosin (HE) staining of retinas in the  $yars2^{+/+}$ ,  $yars2^{+/-}$ , and  $yars2^{-/-}$  zebrafish at 5 dpf. GCL, ganglion cell layer; INL, inner nuclear layer; IPL, inner plexiform layer; ONL, outer nuclear layer; OPL, outer plexiform layer; RPE, retinal pigment epithelium. The angle brackets colored in red denoted the ONL. Scale bar, 50  $\mu$ m. Shorter outer segments in the cones and rods were indicated. *B*, cones and rods in the retinal cross sections of  $yars2^{+/+}$ ,  $yars2^{+/-}$ , and  $yars2^{-/-}$  zebrafish at 5 dpf, stained with lectin PNA-488 (green, yellow arrows) and 1D4/Rhodopsin (red, white arrows) and DAPI (blue) staining for nuclei. Scale bar, 10  $\mu$ m.

the frozen sections of retina in the  $yars2^{-/-}$ ,  $yars2^{+/-}$ , and  $yars2^{+/+}$  larvae at 5 dpf. As shown in Figure 9, A and B, markedly reduced staining of COX but mildly decreased staining of SDH were observed in  $yars2^{-/-}$ , as compared with those in the  $yars2^{+/+}$  larvae. However, the activities of COX and SDH in  $yars2^{-/-}$  were much lower than those in  $yars2^{+/-}$ . These results indicated that the loss of *yars2* caused the pronounced deficiency of complex IV.

Mitochondrial defects in the retina of larvae at 5 dpf were further evaluated by using transmission electron microscope. Mitochondria were usually confined solely to the ellipsoid region of photoreceptors in the zebrafish (48). As shown in Figure 9, C and D, the photoreceptor cells and retinal ganglion cells (RGC) in the  $yars2^{-/-}$  zebrafish displayed less numbers and abnormal morphology of mitochondria, including enlarged mitochondria and the partial loss of cristae, as compared with those in the  $yars2^{+/+}$  larvae. As shown in Figure 9, C and E, mitochondrial numbers of photoreceptor cells in the  $yars2^{-/-}$  ( $n = 25$ ) and  $yars2^{+/-}$  ( $n = 20$ ) mutant larvae were 52% and 92%, related to the mean values of

$yars2^{+/+}$  larvae ( $n = 20$ ), respectively. As shown in Figure 9, D and F, mitochondrial numbers of RGC cells in the  $yars2^{-/-}$  ( $n = 25$ ) and  $yars2^{+/-}$  ( $n = 24$ ) zebrafish larvae were 77% and 108%, related to the average values of those in  $yars2^{+/+}$  larvae ( $n = 32$ ), respectively.

## Discussion

### The impacts of YARS2 on the mitochondrial translation and the stability of OXPHOS

YARS2, like other human mitochondrial tRNA synthetases, has a central role in the aminoacylation of tRNA<sup>Tyr</sup> and mitochondrial translation. In fact, human cytoplasmic aminoacyl-tRNA synthetases have a number of noncanonical functions, including transcriptional regulation, inflammation, angiogenesis, apoptosis, and mitochondrial bioenergetics (11–13, 49, 50). These aminoacyl-tRNA synthetases were present in a free form or part of a high-molecular-weight multisynthetase complex and three scaffold proteins (11, 51). However, the nontranslational functions of human

## Critical roles of mitochondrial tyrosyl-tRNA synthetase

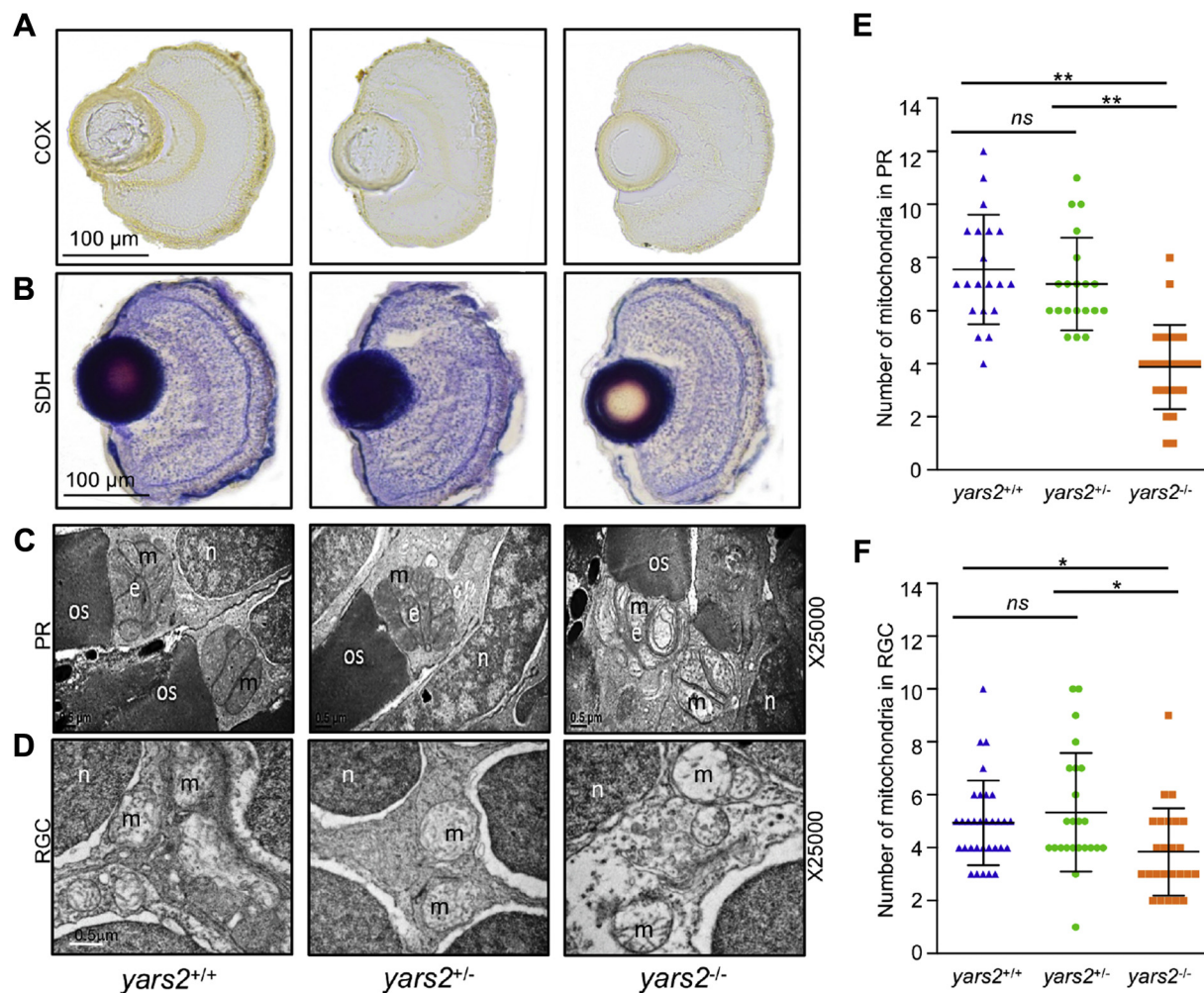


**Figure 9. Mitochondrial defects in the zebrafish retina.** *A* and *B*, assessment of mitochondrial function in the retina by enzyme histochemistry (EHC) staining for COX (*A*) and SDH (*B*) in the frozen sections of retina in the *yars2*<sup>+/+</sup>, *yars2*<sup>+/-</sup>, and *yars2*<sup>-/-</sup> larvae at 5 dpf. Scale bar, 100  $\mu$ m. *C* and *D*, mitochondrial morphology from photoreceptors (PR) (*C*) and RGC (*D*) of transmission electron microscopy. Ultrathin sections were visualized with 25,000 $\times$  magnification. Scale bar, 1  $\mu$ m. e, ellipsoid; m, mitochondrion; n, nucleus; os, outer segment of photoreceptors. *E* and *F*, quantification of mitochondrial numbers of photoreceptors (*E*) from *yars2*<sup>+/+</sup> (*n* = 20), *yars2*<sup>+/-</sup> (*n* = 20), and *yars2*<sup>-/-</sup> (*n* = 25) and RGC (*F*) from *yars2*<sup>+/+</sup> (*n* = 32), *yars2*<sup>+/-</sup> (*n* = 24), and *yars2*<sup>-/-</sup> (*n* = 25) zebrafish at 5 dpf. Graph details and symbols are explained in the legend to [Figure 2](#).

mitochondrial aminoacyl-tRNA synthetases remain poorly understood. In the present investigation, we demonstrated that the YARS2 deficiency caused the pleiotropic effects in the HeLa mutant cells: impairment of mitochondrial translation and instability of OXPHOS complexes. As expected, the primary defects in the YARS2 deficiencies were the aberrant aminoacylation of tRNA<sup>Tyr</sup> and impaired synthesis of mtDNA-encoding 13 OXPHOS subunits (24, 29, 31, 32). The reduced levels among 13 mtDNA-encoding OXPHOS subunits in the cells bearing the YARS2 mutations or deletions were correlated with the tyrosine codon usages of polypeptides, especially marked reductions in the ND1, ND4, ND5, ND6, CO1, and CO2 with high contents of tyrosine codon (24, 29, 31, 32). Strikingly, YARS2 mutant cells displayed various reductions in nucleus-encoding OXPHOS subunits, NDUFS1, NDUFS3, NDUFA9, NDUFB8, SDHB, UQCRC1, UQCRC2, COX5A, and COX16. The mitochondrial translational defects may result in the imbalances between the increased levels of *de novo* protein synthesis and decreased folding capacity for the

mtDNA- and nucleus-encoded mitochondrial proteins (52, 53). It was worthwhile to note that YARS2 deficiency impaired mitochondrial proteostasis, evidenced by the decreased levels of Clpp and LONP1 in the YARS2<sup>KO</sup> cells. Furthermore, the ablation of YARS2 could affect the association of YARS2 and mRNA and regulate the translation of nucleus-encoding OXPHOS subunits (54). Alternatively, YARS2 may interact with NDUFS1, NDUFA9 of complex I and CO2 of complex IV to provide further stabilization of OXPHOS complexes (41, 55, 56). Notably, WARS2 deficiency abolished its interaction with COX11 and led to noncanonical effects on mitochondrial function (57). These deficiencies gave rise to the instability of complexes I, II, III, IV, and V as well as intact supercomplexes observed in YARS2<sup>-/-</sup> cell lines. In fact, each OXPHOS complex is a multisubunit machine integrated into the mitochondrial inner membrane, comprising mtDNA-encoded subunit(s) and nuclear-encoded subunits, except complex II (56). These mtDNA-encoded subunits appear to act as seeds for building new complexes, which requires nuclear-encoded

subunit import and assembly with the assistance of assembly factors (55, 56). As a consequence, these defects yielded the reduced activities of these respiratory chain enzyme complexes. Strikingly, the variations in the average lower concentrations of OXPHOS (complexes I, II, III, IV, and V) proteins in the *YARS2*<sup>KO</sup> line showed a significant correlation with the variations in the reduced activities in the respiratory chain complexes ( $r = 0.98$ ,  $p = 0.0034$ ) (Fig. S6). Therefore, our data demonstrated that *YARS2* has profound impacts on the stability of OXPHOS complexes.

### The critical role of *YARS2* in the vision function

The retina is a part of the central nervous system and shares the characteristically high metabolism of the brain (58, 59). In particular, the photoreceptor cells and RGCs are the biggest ATP demand cells in the retina (58, 60). In fact, aberrant mitochondrial tRNA metabolism, caused by mutations in mitochondrial tRNA or mitochondrial tRNA synthetases, is associated with visual impairment as sole phenotype or associated with other clinical presentations (31, 61–65). Notably, defects in mt-aarSs resulted in the respiratory deficiency, deficient ATP synthesis, and subsequent failure of cellular energetic process (14, 15). In fact, inhibition of *wars2* resulted in trunk vessel deficiencies, disordered endocardial–myocardial contact, and impaired heart function in the zebrafish (57). In this study, it was hypothesized that the mitochondrial dysfunctions caused by *YARS2* deficiency particularly ablated the function of retina in zebrafish. These mitochondrial dysfunctions were evidenced by pronounced reduced activities of COX in the retina, abnormal morphology, and reduced numbers of mitochondria in the photoreceptor cells and RGCs of *yars2*<sup>-/-</sup> mutant zebrafish. Indeed, zebrafish at 5 dpf have functional retina, composed of five layers (ONL, OPL, INL, IPL, and GCL) (45, 46). These mitochondrial dysfunctions caused by the deletion of *yars2* led to the pathological consequence of vision function. At 5 dpf, *yars2*<sup>-/-</sup> mutant larvae exhibited significant decreases in the average area and length of eyes, indicating that the loss of *Yars2* altered the embryonic eye development. The vision deficiencies were further evidenced by the fact that the *yars2*<sup>-/-</sup> mutant zebrafish exhibited the reduced thickness of ONL containing the rod and cone granules: photoreceptor cells. Furthermore, *yars2*<sup>-/-</sup> larvae displayed shortened outer segments of cones and rods, indicating that the loss of *yars2* affected the development and functions of cones and rods. Therefore, we demonstrated that the *yars2* deficiency led to the retinal defects, as in the case of tissue-specific effects in the *DARS2* and *WARS2* mutations (52, 53).

In summary, our findings demonstrated that *YARS2* has the critical roles in the OXPHOS stability and vision functions. Aside from its central function in the mitochondrial protein synthesis, *YARS2* may regulate the mitochondrial proteostasis and activity of OXPHOS complexes *via* its potential interacting with NDUFS1, NDUFA9, and CO2. The mitochondrial dysfunctions

induced by the loss of *Yars2* led to the alterations in the eye development and retina defects in the zebrafish. Our findings highlight the critical roles of mitochondrial aminoacyl-tRNA synthetase in the stability and activity of OXPHOS complex and their pathological consequences in visual impairment.

### Experimental procedures

#### Generation of *YARS2*<sup>KO</sup> HeLa cell line and culture condition

The HeLa cell lines were grown in Dulbecco's Modified Eagle Medium (DMEM) (Life Technologies) (containing 4.5 mg of glucose, 0.11 mg pyruvate/ml, and 50 µg of uridine/ml), supplemented with 5% FBS. Lymphoblastoid cell lines (I-1) bearing the homozygous *YARS2* p.191Gly>Val mutation and control (A61) lacking these mutations were grown in the RPMI 1640 medium (Invitrogen) supplemented with 10% fetal bovine serum (32).

*YARS2*<sup>KO</sup> HeLa cell lines were generated by utilizing the Lenti CRISPR 458 plasmid (Addgene) containing the sgRNAs (66). sgRNAs were designed using the CRISPR design tool (<http://crispr.mit.edu>) to minimize potential off-target effects. The sequences of sgRNAs that ultimately produced successful deletion clones were 5' CAGGAAAAGGACCGCAAGAT3'. HeLa cells were transfected with Lenti CRISPR 458 plasmid (Addgene) containing the sgRNAs using jetPRIME (Polyplus-transfection SA, Illkirch, France), according to the manufacturer's instructions. After 24 h, the cell cultures in the same media were treated with 1 µg/ml of puromycin for 3 days. The cells were then collected and plated in DMEM (containing 4.5 mg of glucose, 0.11 mg pyruvate/ml, and 50 µg of uridine/ml), supplemented with 10% FBS. Subsequently, cells were cloned by limiting dilution, and individual clones were isolated.

Fragments spanning five exons and flanking sequences in each clone were PCR amplified, purified, and subsequently analyzed by Sanger sequencing, as detailed previously (31). These sequence results were compared with the *YARS* genomic sequence (RefSeq NC\_000012.12). The genotyping for the *YARS2*<sup>14bpdel</sup> mutation in each clones was PCR amplified for 354 bp fragment spanning partial promoter region and exon 1 and followed by Sanger sequence analysis and subsequently RFLP analysis by the digestion of *BstNI*. In fact, the *YARS2*<sup>14bpdel</sup> mutation abolished the site of *BstNI* in this fragment. The forward and reverse primers for this genotyping analysis were 5'-ACCTTCCCTAGGAGCTGTAAGTAG-3' and 5'AGATGACCCACATGAAGCGAGTC-3', respectively.

For the rescuing of *YARS2*<sup>KO</sup> cells, the full-length coding region of *YARS2* cDNA was obtained by RT-PCR amplification using the high-fidelity *Pfu* DNA polymerase (Promega) and total RNA isolated from HeLa cells as template, with primers with *EcoRI* site: 5'-GGAATTCCATGGCGGCGCCCAT-3'(nt.24–38) and *BamHI* site: CGGGATCCCGTCA-CAACTGAAGCCATTTTATAA-3'(nt.1435–1457) (GenBank accession no. NM\_001040436.3) (67). The PCR products were cloned by using the TA Cloning Kit (TAKARA) and analyzed by Sanger sequencing and then subcloned into a

## Critical roles of mitochondrial tyrosyl-tRNA synthetase

pCDH-puro-cMyc Vector (Addgene plasmid 46970). The YARS2<sup>KO</sup> HeLa cell lines were transfected with pCDH-puro-cMyc Vector with YARS2 cDNA, pMD2.G (Addgene), and psPAX2 (Addgene) plasmids in DMEM (10569-010) using Lipofectamine 3000 (Life Technologies) (68, 69).

### Mitochondrial tRNA analysis

Total RNAs were obtained from HeLa cell lines (~1.0 × 10<sup>8</sup> cells), as described previously (70). For tRNA aminoacylation analysis, 10 µg of total RNAs was electrophoresed at 4 °C through an acid (pH 5.2) 10% polyacrylamide/8 M urea gel to separate the charged and uncharged tRNA as detailed elsewhere (71–73). The gels were electroblotted onto a positively charged nylon membrane (Roche) for the hybridization analysis with oligodeoxynucleotide probes specific tRNA<sup>Tyr</sup>, tRNA<sup>Leu(UUR)</sup>, and tRNA<sup>Thr</sup>, as detailed elsewhere (71–73).

### Experimental fish and maintenance

AB wild-type strain and myocardium-specific transgenic *Tg* (*cmlc2: egfp*) zebrafish (*Danio rerio*) were used for this investigation. The animal protocols used in this investigation were approved by the Zhejiang University Institutional Animal Care and Use Committee. All fishes were kept in recirculating water at 28 °C and fed with commercial pellets at a daily ration of 0.7% of their body weight. Embryos were reared at 28.5 °C according to standard protocols (74). Embryos were staged by hours post fertilization (hpf) and days post fertilization (dpf) (75).

### Yars2-knockout zebrafish line generated by CRISPR/Cas9 system

The zCas9 expression plasmid pSP6-2sNLS-spCas9 was linearized by *Xba* I and used as a template for Cas9 mRNA *in vitro* synthesis with mMACHINE mRNA transcription synthesis kits (Ambion). The sequence of sgRNAs was designed according to criteria as described previously (66, 76). The gRNA transcription plasmid was pT7-gRNA. We used the CRISPR/Cas9 design tool (<http://zifit.partners.org>) to select specific targets to minimize off-target effects. The sequences of sgRNAs that ultimately produced successful deletion clones were: 5'GGACTCTTCCCG-GAGGTCGCGG3' (GenBank accession no. NM\_001143920.1). Cas9-encoding mRNA (300 ng/µl) and gRNA (200 ng/µl) were coinjected into one-cell-stage wild-type embryos. Injected embryos were incubated at 28.5 °C and collected for making genomic DNA for genotyping at 50 hpf. Genomic DNA of the 50 hpf injected embryo was used as template to amplify DNA segments carrying the partial exo1 sequence in the *yars2* carrying the 5 bp deletion at position 117 by using the following two primers: 5'-AAA-CATCCGCCAAACCTCCC-3' (forward) and 5'-AGGA-GACCCCGGTTATGGAG-3' (reverse) (GenBank accession no. NM\_001143920.1). The genotyping for the *yars2*<sup>5bpdel</sup> mutation in each fish was PCR amplified for 170 bp fragment in the partial exon 1 and followed by Sanger sequence analysis

and subsequently PAGE analysis. The forward and reverse primers for this genotyping analysis were described as above.

### Western blotting analysis

Western blot analysis was performed on samples from the human cell lines and zebrafish larvae at 5 dpf, as detailed elsewhere (31, 32, 43). Fishes were sacrificed after anesthesia and homogenized in RIPA reagent (Invitrogen) using a homogenizer. In total, 20 µg of proteins was electrophoresed through 10% bis-Tris SDS-polyacrylamide gels and then transferred to a polyvinylidene difluoride membrane. The antibodies used for this investigation were from Abcam [YARS2 (ab127542), ND6 (ab81212), NDUFB8 (ab110242), TOM20 (ab56783), SDHB(ab14714), UQCRC2 (ab14745), total human OXPHOS antibody cocktail (ab110411)], Proteintech [NDUFS1 (12444-1-AP), NDUFA9 (20312-1-AP), NDUFS3 (15066-1-AP), SDHA (14865-1-AP), CYTB (55090-1AP), UQCRC1 (21705-1-AP), CO2 (55070-1-AP), COX17 (11464-1-AP), COX16 (19425-1-AP), COX10 (10611-2-AP), COX5A (11448-1-AP), ATP8 (26723-1-AP), ATP5C (10910-1-AP), ATP5F1 (15999-1-AP) and Clpp (15698-1-AP)], LONP1 (15440-1-AP) and COX4 (diagbio, db15), GAPDH (Hangzhou Goodhere Biotechnology Co, Ltd, AB-M-M 001), Anti-HA antibody (Rakland, 600-401-334), and Flag-tagged monoclonal antibody (GNI, GNI4110)]. Peroxidase Affini Pure goat anti-mouse IgG and goat anti-rabbit IgG (Jackson) were used as a secondary antibody. Quantification of density in each band was performed as detailed previously (31).

### Immunoprecipitation analysis

The pcDNA3.1-FLAG and pcDNA3.1-HA constructs were gifts from Dr E. Wang (Chinese Academy of Sciences). The human YARS2 cDNAs were cloned into the pcDNA3.1-FLAG and pcDNA3.1-HA vector. The human NDUFA9 cDNA was amplified with primers: 5'- GG AATTC-CATGGCGGCTGCCGCA-3' (forward) and 5'- GGCGA-TATCGCCAAATG TTGACGGTCTTGCCG-3' (reverse) and cloned into the pcDNA3.1-FLAG vector. HeLa cells were transfected with constructs using jetPRIME (Polyplus -transfection SA). After transfection for 24 h, the cells were collected, washed by phosphate-buffered saline (PBS), and lysed with 1 ml of ice-cold lysis buffer [50 mM Tris-HCl (pH 7.5), 150 mM NaCl, 0.5% (w/v) sodium deoxycholate, 1%(v/v) NP-40] supplemented with a protease inhibitor cocktail (B14001, Selleck) for 15 min on ice. The whole-cell lysates were collected by centrifugation at 12,000g for 30 min at 4 °C and incubated with anti-FLAG tag monoclonal antibody (GNI4110, GNI) or CO2, or NDUFS1 overnight at 4 °C. The Protein A-Agarose beads (Roche) were washed four times with 1 ml of cold PBS buffer (pH 7.4). The beads-bound proteins were eluted and denatured with an SDS loading buffer and subjected to SDS-PAGE and western blot analyses (77, 78).

### Blue native electrophoresis analysis

Blue native gel electrophoresis was performed by isolating mitochondrial proteins from various cell lines, as detailed

previously (35, 36). Samples containing 30 µg of mitochondrial proteins were separated on 3 to 11% Bis-Tris Native PAGE gel. The primary antibodies applied for this experiment were total human OXPHOS antibody cocktail and TOM20 as a loading control. Alkaline phosphatase labeled goat anti-mouse IgG and goat anti-rabbit IgG (Beyotime) were used as secondary antibodies and protein signals were detected using BCIP/NBT alkaline phosphatase color development kit (Beyotime).

### Assays of activities of OXPHOS complexes

For evaluating the activity of complexes I, II, and IV in gel, 30 µg of freshly prepared mitochondrial proteins from various cell lines was loaded on 3 to 11% Bis-Tris Native PAGE gel, run at 150 V in dark blue cathode buffer for 1 h, and then at 250 V in light cathode buffer for 2 h. The native gels were prewashed in cold water and then incubated with the substrate of with the fresh substrates of complex I [0.1 mg/ml NADH, 2.5 mg/ml Nitrotetrazolium Blue chloride (NTB), 2 mM Tris-HCl, pH 7.4], complex II (20 mM sodium succinate, 2.5 mg/ml NTB, 0.2 mM phenazine methosulfate, 5 mM Tris-HCl, pH 7.4), and complex IV [0.5 mg/ml diaminobenzidine (DAB), 1 mg/ml cytochrome c, 45 mM phosphate buffer, pH 7.4] for 2 h at room temperature, respectively. The gel was washed with 50% methanol three times (36–38).

EHC staining for SDH and COX in the frozen sections from *yars2<sup>+/-</sup>*, *yars2<sup>-/-</sup>*, and WT zebrafish larvae at 5 dpf was performed as detailed elsewhere (44, 78). Briefly, freshly dissected retina tissues were embedded in OCT compound (Tissue-Tek), frozen on dry ice, and sectioned to 8 µm. For SDH staining, samples were incubated in 0.1 M phosphate buffer, pH 7.6, containing 5 mM EDTA, 1 mM potassium cyanide, 0.2 mM phenazine methosulfate, 50 mM succinic acid, 1.5 mM nitro blue tetrazolium at 37 °C for 25 min. For COX staining, samples were incubated in 5 mM phosphate buffer, pH 7.6, containing 5 mM EDTA, 1 mM potassium cyanide, 0.2 mM phenazine methosulfate, 50 mM succinic acid, 1.5 mM nitro blue tetrazolium at 37 °C for 60 min.

### Hematoxylin and eosin (H&E) staining

For H&E staining, zebrafish larvae at 5 dpf were anesthetized and fixed in 4% paraformaldehyde with 0.1 M phosphate buffer (PFA) for 24 h at room temperature. Retinal sections were then dehydrated, infiltrated, embedded in paraffin, sliced 3 µm thick by pathologic microtome (RM2016, Leica), and finally stained with H&E (Thermo) to observe tissue architectures (78–80).

### Immunohistochemistry

Zebrafish larvae at 5 dpf were fixed with 4% PFA and permeabilized with 0.01% Triton X-100. Retinal sections were cryoprotected in 8 µM and dried onto frost-free slides at 37 °C overnight, and next blocked (1% BSA, 5% normal goat serum, 0.2% Triton-X-100, 0.1% Tween-20 in 1X PBS) in a humidified chamber for 2 h. Cones and rods OS were labeled respectively with anti-1D4/Rhodopsin (1:250, Abcam ab5417) and

anti-lectin PNA-488 (1:2000, Molecular Probes L21409) antibodies overnight at 4 °C.

### Transmission electron microscopy

The ultrastructure of zebrafish retina at 5 dpf was observed using transmission electron microscopy (47). Retina tissues were fixed in 2.5% glutaraldehyde, embedded in Epon 812, and cut into 100-nm-thick slices using UC7 ultramicrotome (Leica), then stained with 2% uranyl acetate and alkaline lead citrate. Finally, the images of retina ultrastructure were captured by a Hitachi-7650 transmission electron microscope (Hitachi).

### Statistical analysis

All statistical analysis was performed using the unpaired, two-tailed Student's *t*-test contained in the Graphpad prism 8 program (Graphpad software) and Microsoft-Excel program (version 2016). A *p* value <0.05 was considered statistically significant.

### Data availability

Representative experiments are shown in the figures and supplemental materials. For any additional information, please contact the corresponding author.

*Supporting information*—This article contains [supporting information](#).

*Author contributions*—M.-X. G. and P. J. designed the experiments, monitored the project progression, data analysis, and interpretation. X. J., Z. N., C. W., F. M., and Q. Y. contributed to the experiments and contributed to data analysis [Figures 1–5](#). Z. Z., M. C., J. S., and J. Z. performed the experiments and contributed to data analysis in [Figures 6–8](#). P. J. and M.-X. G. acquired funds. P. J. prepared the initial draft of the article. M.-X. G. made the final version of the article. All the authors reviewed the article.

*Funding and additional information*—This work was supported by a grant from the National Key Research and Development Program of China, China (2018YFC1004802 to M.-X. G.), grants from National Natural Science Foundation of China, China (31970557 to M.-X. G., 31671303 to P. J.) and Zhejiang Provincial Medical and Health Research Program, China (2019RC149 to X. J.).

*Conflict of interest*—All the authors declare that they have no conflict of interest with the contents of this article.

*Abbreviations*—The abbreviations used are: DMEM, Dulbecco's modified eagle medium; EHC, enzyme histochemistry; GCL, ganglion cell layer; H&E, hematoxylin and eosin; INL, inner nuclear layer; IPL, inner plexiform layer; KO, knockout; MLASA, myopathy, lactic acidosis, and sideroblastic anemia; mtDNA, mitochondrial DNA; OCR, oxygen consumption rate; ONL, outer nuclear layer; OPL, outer plexiform layer; OXPHOS, oxidative phosphorylation system.

# Critical roles of mitochondrial tyrosyl-tRNA synthetase

## References

- Wallace, D. C. (2018) Mitochondrial genetic medicine. *Nat. Genet.* **50**, 1642–1649
- Craven, L., Alston, C. L., Taylor, R. W., and Turnbull, D. M. (2017) Recent advances in mitochondrial disease. *Annu. Rev. Genomics Hum. Genet.* **18**, 257–275
- DiMauro, S., and Schon, E. A. (2008) Mitochondrial disorders in the nervous system. *Annu. Rev. Neurosci.* **31**, 91–123
- Suzuki, T., Nagao, A., and Suzuki, T. (2011) Human mitochondrial tRNAs: Biogenesis, function, structural aspects, and diseases. *Annu. Rev. Genet.* **45**, 299–329
- Guan, M. X. (2011) Mitochondrial 12S rRNA mutations associated with aminoglycoside ototoxicity. *Mitochondrion* **11**, 237–245
- Boczonadi, V., Ricci, G., and Horvath, R. (2018) Mitochondrial DNA transcription and translation: Clinical syndromes. *Essays Biochem.* **62**, 321–340
- Meng, F., Zhou, M., Xiao, Y., Mao, X., Zheng, J., Lin, J., Lin, T., Ye, Z., Cang, X., Fu, Y., Wang, M., and Guan, M. X. (2021) A deafness-associated tRNA mutation caused pleiotropic effects on the m<sup>1</sup>G37 modification, processing, stability and aminoacylation of tRNA<sup>Leu</sup> and mitochondrial translation. *Nucleic Acids Res.* **49**, 1075–1093
- Sissler, M., González-Serrano, L. E., and Westhof, E. (2017) Recent advances in mitochondrial aminoacyl-tRNA synthetases and disease. *Trends Mol. Med.* **23**, 693–708
- Fine, A. S., Nemeth, C. L., Kaufman, M. L., and Fatemi, A. (2019) Mitochondrial aminoacyl-tRNA synthetase disorders: An emerging group of developmental disorders of myelination. *J. Neurodev. Disord.* **11**, 29
- Ognjenović, J., and Simonović, M. (2018) Human aminoacyl-tRNA synthetases in diseases of the nervous system. *RNA Biol.* **15**, 623–634
- Guo, M., and Schimmel, P. (2013) Essential nontranslational functions of tRNA synthetases. *Nat. Chem. Biol.* **9**, 145–153
- Fang, P., and Guo, M. (2017) Structural characterization of human aminoacyl-tRNA synthetases for translational and nontranslational functions. *Methods* **113**, 83–90
- Son, K., You, J. S., Yoon, M. S., Dai, C., Kim, J. H., Khanna, N., Banerjee, A., Martinis, S. A., Han, G., Han, J. M., Kim, S., and Chen, J. (2019) Nontranslational function of leucyl-tRNA synthetase regulates myogenic differentiation and skeletal muscle regeneration. *J. Clin. Invest.* **129**, 2088–2093
- González-Serrano, L. E., Chihade, J. W., and Sissler, M. (2019) When a common biological role does not imply common disease outcomes: Disparate pathology linked to human mitochondrial aminoacyl-tRNA synthetases. *J. Biol. Chem.* **294**, 5309–5320
- Tynnismaa, H., and Schon, E. A. (2014) Mixing and matching mitochondrial aminoacyl synthetases and their tRNAs: A new way to treat respiratory chain disorders? *EMBO Mol. Med.* **6**, 155–157
- Opreescu, S. N., Griffin, L. B., Beg, A. A., and Antonellis, A. (2017) Predicting the pathogenicity of aminoacyl-tRNA synthetase mutations. *Methods* **113**, 139–151
- Finsterer, J., and Zarrouk-Mahjoub, S. (2017) Phenotypic spectrum of DARS2 mutations. *J. Neurol. Sci.* **376**, 117–118
- Steenweg, M. E., Ghezzi, D., Haack, T., Abbink, T. E., Martinelli, D., van Berkel, C. G., Bley, A., Diogo, L., Grillo, E., Te Water Naudé, J., Strom, T. M., Bertini, E., Prokisch, H., van der Knaap, M. S., and Zeviani, M. (2012) Leukoencephalopathy with thalamus and brainstem involvement and high lactate 'LTBL' caused by EARS2 mutations. *Brain* **135**, 1387–1394
- Simon, M., Richard, E. M., Wang, X., Shahzad, M., Huang, V. H., Qaiser, T. A., Potluri, P., Mahl, S. E., Davila, A., Nazli, S., Hancock, S., Yu, M., Gargus, J., Chang, R., Al-Sheqaih, N., et al. (2015) Mutations of human NARS2, encoding the mitochondrial asparaginyl-tRNA synthetase, cause nonsyndromic deafness and Leigh syndrome. *PLoS Genet.* **11**, e1005097
- Pierce, S. B., Gersak, K., Michaelson-Cohen, R., Walsh, T., Lee, M. K., Malach, D., Klevit, R. E., King, M. C., and Levy-Lahad, E. (2013) Mutations in LARS2, encoding mitochondrial leucyl-tRNA synthetase, lead to premature ovarian failure and hearing loss in Perrault syndrome. *Am. J. Hum. Genet.* **92**, 614–620
- Diodato, D., Melchionda, L., Haack, T. B., Dallabona, C., Baruffini, E., Donnini, C., Granata, T., Ragona, F., Balestri, P., Margollicci, M., Lamantea, E., Nasca, A., Powell, C. A., Minczuk, M., Strom, T. M., et al. (2014) VARS2 and TARS2 mutations in patients with mitochondrial encephalomyopathies. *Hum. Mutat.* **35**, 983–989
- McMillan, H. J., Humphreys, P., Smith, A., Schwartzentruber, J., Chakraborty, P., Bulman, D. E., Beaulieu, C. L., Majewski, J., Boycott, K. M., and Geraghty, M. T. (2015) Congenital visual impairment and progressive microcephaly due to lysyl-transfer ribonucleic acid (RNA) synthetase (KARS) mutations: The expanding phenotype of aminoacyl-transfer RNA synthetase mutations in human disease. *J. Child. Neurol.* **30**, 1037–1043
- Coughlin, C. R., Scharer, G. H., Friederich, M. W., Yu, H. C., Geiger, E. A., Creadon-Swindell, G., Collins, A. E., Vanlander, A. V., Coster, R. V., Powell, C. A., Swanson, M. A., Minczuk, M., Van Hove, J. L., and Shaikh, T. H. (2015) Mutations in the mitochondrial cysteinyl-tRNA synthase gene, CARS2, lead to a severe epileptic encephalopathy and complex movement disorder. *J. Med. Genet.* **52**, 532–540
- Riley, L. G., Cooper, S., Hickey, P., Rudinger-Thirion, J., McKenzie, M., Compton, A., Lim, S. C., Thorburn, D., Ryan, M. T., Giegé, R., Bahlo, M., and Christodoulou, J. (2010) Mutation of the mitochondrial tyrosyl-tRNA synthetase gene, YARS2, causes myopathy, lactic acidosis, and sideroblastic anemia—MLASA syndrome. *Am. J. Hum. Genet.* **87**, 52–59
- Sommerville, E. W., Ng, Y. S., Alston, C. L., Dallabona, C., Gilberti, M., He, L., Knowles, C., Chin, S. L., Schaefer, A. M., Falkous, G., Murdoch, D., Longman, C., de Visser, M., Bindoff, L. A., Rawles, J. M., et al. (2017) Clinical features, molecular heterogeneity, and prognostic implications in YARS2-related mitochondrial myopathy. *JAMA Neurol.* **74**, 686–694
- Nakajima, J., Eminoglu, T. F., Vatansever, G., Nakashima, M., Tsurusaki, Y., Saitou, H., Kawashima, H., Matsumoto, N., and Miyake, N. (2014) A novel homozygous YARS2 mutation causes severe myopathy, lactic acidosis, and sideroblastic anemia 2. *J. Hum. Genet.* **59**, 229–232
- Shahni, R., Wedatilake, Y., Cleary, M. A., Lindley, K. J., Sibson, K. R., and Rahman, S. (2013) A distinct mitochondrial myopathy, lactic acidosis and sideroblastic anemia (MLASA) phenotype associates with YARS2 mutations. *Am. J. Med. Genet. A* **161A**, 2334–2338
- Riley, L. G., Heaney, M. M., Rudinger-Thirion, J., Frugier, M., Campagna, D. R., Zhou, R., Hale, G. A., Hilliard, L. M., Kaplan, J. A., Kwiatkowski, J. L., Sieff, C. A., Steensma, D. P., Rennings, A. J., Simons, A., Schaap, N., et al. (2018) The phenotypic spectrum of germline YARS2 variants: From isolated sideroblastic anemia to mitochondrial myopathy, lactic acidosis and sideroblastic anemia 2. *Haematologica* **103**, 2008–2015
- Sasarman, F., Nishimura, T., Thiffault, I., and Shoubridge, E. A. (2012) A novel mutation in YARS2 causes myopathy with lactic acidosis and sideroblastic anemia. *Hum. Mutat.* **33**, 1201–1206
- Riley, L. G., Menezes, M. J., Rudinger-Thirion, J., Duff, R., de Lonlay, P., Rotig, A., Tchan, M. C., Davis, M., Cooper, S. T., and Christodoulou, J. (2013) Phenotypic variability and identification of novel YARS2 mutations in YARS2 mitochondrial myopathy, lactic acidosis and sideroblastic anaemia. *Orphanet. J. Rare Dis.* **8**, 193
- Jiang, P., Jin, X., Peng, Y., Wang, M., Liu, H., Liu, X., Zhang, Z., Ji, Y., Zhang, J., Liang, M., Zhao, F., Sun, Y. H., Zhang, M., Zhou, X., Chen, Y., et al. (2016) The exome sequencing identified the mutation in YARS2 encoding the mitochondrial tyrosyl-tRNA synthetase as a nuclear modifier for the phenotypic manifestation of Leber's hereditary optic neuropathy-associated mitochondrial DNA mutation. *Hum. Mol. Genet.* **25**, 584–596
- Fan, W., Zheng, J., Kong, W., Cui, L., Aishanjiang, M., Yi, Q., Wang, M., Cang, X., Tang, X., Chen, Y., Mo, J. Q., Sondheimer, N., Ge, W., and Guan, M. X. (2019) Contribution of a mitochondrial tyrosyl-tRNA synthetase mutation to the phenotypic expression of the deafness-associated tRNA<sup>Ser(UCN)</sup> 7511A>G mutation. *J. Biol. Chem.* **294**, 19292–19305
- Szczepanowska, K., Maiti, P., Kukut, A., Hofsetz, E., Nolte, H., Senft, K., Becker, C., Ruzzenente, B., Hornig-Do, H. T., Wibom, R., Wiesner, R. J., Krüger, M., and Trifunovic, A. (2016) CLPP coordinates mitoribosomal assembly through the regulation of ERAL1 levels. *EMBO J.* **35**, 2566–2583
- Truscott, K. N., Lowth, B. R., Strack, P. R., and Dougan, D. A. (2010) Diverse functions of mitochondrial AAA+ proteins: Protein activation, disaggregation, and degradation. *Biochem. Cell Biol.* **88**, 97–108

35. Jha, P., Wang, X., and Auwerx, J. (2016) Analysis of mitochondrial respiratory chain super-complexes using blue native polyacrylamide gel electrophoresis (BN-PAGE). *Curr. Protoc. Mouse Biol.* **6**, 1–14
36. Ji, Y., Zhang, J., Yu, J., Wang, Y., Lu, Y., Liang, M., Li, Q., Jin, X., Wei, Y., Meng, F., Gao, Y., Cang, X., Tong, Y., Liu, X., Zhang, M., *et al.* (2019) Contribution of mitochondrial ND1 3394T>C mutation to the phenotypic manifestation of Leber's hereditary optic neuropathy. *Hum. Mol. Genet.* **28**, 1515–1529
37. Birch-Machin, M. A., and Turnbull, D. M. (2001) Assaying mitochondrial respiratory complex activity in mitochondria isolated from human cells and tissues. *Methods Cell Biol.* **65**, 97–117
38. Meng, F., He, Z., Tang, X., Zheng, J., Jin, X., Zhu, Y., Ren, X., Zhou, M., Wang, M., Gong, S., Mo, J. Q., Shu, Q., and Guan, M. X. (2018) Contribution of the tRNA<sup>Leu</sup> 4317A>G mutation to the phenotypic manifestation of the deafness-associated mitochondrial 12S rRNA 1555A>G mutation. *J. Biol. Chem.* **293**, 3321–3334
39. Dranka, B. P., Benavides, G. A., Diers, A. R., Giordano, S., Zelickson, B. R., Reily, C., Zou, L., Chatham, J. C., Hill, B. G., Zhang, J., Landar, A., and Darley-Usmar, V. M. (2011) Assessing bioenergetic function in response to oxidative stress by metabolic profiling. *Free Radic. Biol. Med.* **51**, 1621–1635
40. Gong, S., Peng, Y., Jiang, P., Wang, M., Fan, M., Wang, X., Zhou, H., Li, H., Yan, Q., Huang, T., and Guan, M. X. (2014) A deafness-associated tRNA<sup>His</sup> mutation alters the mitochondrial function, ROS production and membrane potential. *Nucleic Acids Res.* **42**, 8039–8048
41. Guo, R., Zong, S., Wu, M., Gu, J., and Yang, M. (2017) Architecture of human mitochondrial respiratory megacomplex I<sub>2</sub>III<sub>2</sub>IV<sub>2</sub>. *Cell* **170**, 1247–1257.e1212
42. Bonnefond, L., Frugier, M., Touze, E., Lorber, B., Florentz, C., Giege, R., Sauter, C., and Rudinger-Thirion, J. (2007) Crystal structure of human mitochondrial tyrosyl-tRNA synthetase reveals common and idiosyncratic features. *Structure* **15**, 1505–1516
43. Chen, D., Zhang, Z., Chen, C., Yao, S., Yang, Q., Li, F., He, X., Ai, C., Wang, M., and Guan, M. X. (2019) Deletion of Gtpbp3 in zebrafish revealed the hypertrophic cardiomyopathy manifested by aberrant mitochondrial tRNA metabolism. *Nucleic Acids Res.* **47**, 5341–5355
44. Zhang, Q., Zhang, L., Chen, D., He, X., Yao, S., Zhang, Z., Chen, Y., and Guan, M. X. (2018) Deletion of Mtu1 (Trnu) in Zebrafish revealed the essential role of tRNA modification in mitochondrial biogenesis and hearing function. *Nucleic Acids Res.* **46**, 10930–10945
45. Fadool, J. M., and Dowling, J. E. (2008) Zebrafish: A model system for the study of eye genetics. *Prog. Retin. Eye Res.* **27**, 89–110
46. Coltery, R. F., Veth, K. N., Dubis, A. M., Carroll, J., and Link, B. A. (2014) Rapid, accurate, and non-invasive measurement of Zebrafish axial length and other eye dimensions using SD-OCT allows longitudinal analysis of myopia and emmetropization. *PLoS One* **9**, e110699
47. Liu, Y., Cao, S., Yu, M., and Hu, H. (2020) TMEM216 deletion causes mislocalization of cone opsin and rhodopsin and photoreceptor degeneration in Zebrafish. *Invest. Ophthalmol. Vis. Sci.* **61**, 24
48. Tarboush, R., Chapman, G. B., and Connaughton, V. P. (2012) Ultrastructure of the distal retina of the adult Zebrafish, *Danio Rerio*. *Tissue Cell* **44**, 264–279
49. Park, S. G., Ewalt, K. L., and Kim, S. (2005) Functional expansion of aminoacyl-tRNA synthetases and their interacting factors: New perspectives on housekeepers. *Trends Biochem. Sci.* **30**, 569–574
50. Akaike, T., Ida, T., Wei, F. Y., Nishida, M., Kumagai, Y., Alam, M. M., Ihara, H., Sawa, T., Matsunaga, T., Kasamatsu, S., Nishimura, A., Morita, M., Tomizawa, K., Nishimura, A., Watanabe, S., *et al.* (2017) Cysteinyln-tRNA synthetase governs cysteine polysulfidation and mitochondrial bioenergetics. *Nat. Commun.* **8**, 1177
51. Hyeon, D. Y., Kim, J. H., Ahn, T. J., Cho, Y., Hwang, D., and Kim, S. (2019) Evolution of the multi-tRNA synthetase complex and its role in cancer. *J. Biol. Chem.* **294**, 5340–5351
52. Agnew, T., Goldsworthy, M., Aguilar, C., Morgan, A., Simon, M., Hilton, H., Esapa, C., Wu, Y., Cater, H., Bentley, L., Scudamore, C., Poulton, J., Morten, K. J., Thompson, K., He, L., *et al.* (2018) A Wars2 mutant mouse model displays OXPHOS deficiencies and activation of tissue-specific stress response pathways. *Cell Rep.* **25**, 3315–3328
53. Dogan, S. A., Pujol, C., Maiti, P., Kukut, A., Wang, S., Hermans, S., Senft, K., Wibom, R., Rugarli, E. I., and Trifunovic, A. (2014) Tissue-specific loss of DARS2 activates stress responses independently of respiratory chain deficiency in the heart. *Cell Metab.* **19**, 458–469
54. Levi, O., and Arava, Y. (2019) mRNA association by aminoacyl tRNA synthetase occurs at a putative anticodon mimic and autoregulates translation in response to tRNA levels. *PLoS Biol.* **17**, e3000274
55. Mukherjee, S., and Ghosh, A. (2020) Molecular mechanism of mitochondrial respiratory chain assembly and its relation to mitochondrial diseases. *Mitochondrion* **53**, 1–20
56. Signes, A., and Fernandez-Vizarra, E. (2018) Assembly of mammalian oxidative phosphorylation complexes I-V and supercomplexes. *Essays Biochem.* **62**, 255–270
57. Wang, M., Sips, P., Khin, E., Rotival, M., Sun, X., Ahmed, R., Widjaja, A. A., Schafer, S., Yusoff, P., Choksi, P. K., Ko, N. S., Singh, M. K., Epstein, D., Guan, Y., Houštěk, J., *et al.* (2016) Wars2 is a determinant of angiogenesis. *Nat. Commun.* **7**, 12061
58. Country, M. W. (2017) Retinal metabolism: A comparative look at energetics in the retina. *Brain Res.* **1672**, 50–57
59. Wong-Riley, M. T. (2010) Energy metabolism of the visual system. *Eye Brain* **2**, 99–116
60. Ames, A. (1992) Energy requirements of CNS cells as related to their function and to their vulnerability to ischemia: A commentary based on studies on retina. *Can. J. Physiol. Pharmacol.* **70**, S158–S164
61. Zhang, J., Ji, Y., Liu, X., Chen, J., Wang, B., Zhang, M., and Guan, M. X. (2018) Leber's hereditary optic neuropathy caused by a mutation in mitochondrial tRNA<sup>Thr</sup> in eight Chinese pedigrees. *Mitochondrion* **42**, 84–91
62. Qu, J., Li, R., Tong, Y., Lu, F., Qian, Y., Hu, Y., Mo, J. Q., West, C. E., and Guan, M. X. (2006) The novel A4435G mutation in the mitochondrial tRNA<sup>Met</sup> may modulate the phenotypic expression of the LHON-associated ND4 G11778A mutation in a Chinese family. *Invest. Ophthalmol. Vis. Sci.* **47**, 475–483
63. Smith, P. R., Bain, S. C., Good, P. A., Hattersley, A. T., Barnett, A. H., Gibson, J. M., and Dodson, P. M. (1999) Pigmentary retinal dystrophy and the syndrome of maternally inherited diabetes and deafness caused by the mitochondrial DNA 3243 tRNA<sup>Leu(UUR)</sup> A to G mutation. *Ophthalmology* **106**, 1101–1108
64. Peragallo, J. H., Keller, S., van der Knaap, M. S., Soares, B. P., and Shankar, S. P. (2018) Retinopathy and optic atrophy: Expanding the phenotypic spectrum of pathogenic variants in the AARS2 gene. *Ophthalmic Genet.* **39**, 99–102
65. McMillan, H. J., Humphreys, P., Smith, A., Schwartzentruber, J., Chakraborty, P., Bulman, D. E., Beaulieu, C. L., au, f.m., Majewski, J., Boycott, K. M., and Geraghty, M. T. (2015) Congenital visual impairment and progressive microcephaly due to lysyl-transfer ribonucleic acid (RNA) synthetase (KARS) mutations: The expanding phenotype of aminoacyl-transfer RNA synthetase mutations in human disease. *J. Child. Neurol.* **30**, 1037–1043
66. Shalem, O., Sanjana, N. E., Hartenian, E., Shi, X., Scott, D. A., Mikkelsen, T., Heckl, D., Ebert, B. L., Root, D. E., Doench, J. G., and Zhang, F. (2014) Genome-scale CRISPR-Cas9 knockout screening in human cells. *Science* **343**, 84–87
67. Bonnefond, L., Fender, A., Rudinger-Thirion, J., Giege, R., Florentz, C., and Sissler, M. (2005) Toward the full set of human mitochondrial aminoacyl-tRNA synthetases: Characterization of AspRS and TyrRS. *Biochemistry* **44**, 4805–4816
68. Cheng, Z., Gong, Y., Ma, Y., Lu, K., Lu, X., Pierce, L. A., Thompson, R. C., Muller, S., Knapp, S., and Wang, J. (2013) Inhibition of BET bromodomain targets genetically diverse glioblastoma. *Clin. Cancer Res.* **19**, 1748–1759
69. Rodina, A., Wang, T., Yan, P., Gomes, E. D., Dunphy, M. P., Pillarsetty, N., Koren, J., Gerecitano, J. F., Taldone, T., Zong, H., Caldas-Lopes, E., Alpaugh, M., Corben, A., Riolo, M., Beattie, B., *et al.* (2016) The epichaperome is an integrated chaperome network that facilitates tumour survival. *Nature* **538**, 397–401
70. King, M. P., and Attardi, G. (1993) Post-transcriptional regulation of the steady-state levels of mitochondrial tRNAs in HeLa cells. *J. Biol. Chem.* **268**, 10228–10237

## Critical roles of mitochondrial tyrosyl-tRNA synthetase

71. Enriquez, J. A., and Attardi, G. (1996) Analysis of aminoacylation of human mitochondrial tRNAs. *Methods Enzymol.* **264**, 183–196
72. Jia, Z., Zhang, Y., Li, Q., Ye, Z., Liu, Y., Fu, C., Cang, X., Wang, M., and Guan, M. X. (2019) A coronary artery disease-associated tRNA<sup>Thr</sup> mutation altered mitochondrial function, apoptosis and angiogenesis. *Nucleic Acids Res.* **47**, 2056–2074
73. Zhou, M., Xue, L., Chen, Y., Li, H., He, Q., Wang, B., Meng, F., Wang, M., and Guan, M. X. (2018) A hypertension-associated mitochondrial DNA mutation introduces an m<sup>1</sup>G37 modification into tRNA<sup>Met</sup>, altering its structure and function. *J. Biol. Chem.* **293**, 1425–1438
74. Westerfield, M. (2000) *The Zebrafish Book. A Guide for the Laboratory Use of Zebrafish (Danio rerio)*, University of Oregon Press, Eugene
75. Kimmel, C. B., Ballard, W. W., Kimmel, S. R., Ullmann, B., and Schilling, T. F. (1995) Stages of embryonic development of the Zebrafish. *Dev. Dyn.* **203**, 253–310
76. Gonzales, A. P., and Yeh, J. R. (2014) Cas9-based genome editing in Zebrafish. *Methods Enzymol.* **546**, 377–413
77. Escobar-Alvarez, S., Gardner, J., Sheth, A., Manfredi, G., Yang, G., Ouerfelli, O., Heaney, M. L., and Scheinberg, D. A. (2010) Inhibition of human peptide deformylase disrupts mitochondrial function. *Mol. Cell Biol.* **30**, 5099–5109
78. Yu, J., Liang, X., Ji, Y., Ai, C., Liu, J., Zhu, L., Nie, Z., Jin, X., Wang, C., Zhang, J., Zhao, F., Mei, S., Zhao, X., Zhou, X., Zhang, M., *et al.* (2020) PRICKLE3 linked to ATPase biogenesis manifested Leber's hereditary optic neuropathy. *J. Clin. Invest.* **130**, 4935–4946
79. Phillips, M. J., Webb-Wood, S., Faulkner, A. E., Jabbar, S. B., Biousse, V., Newman, N. J., Do, V. T., Boatright, J. H., Wallace, D. C., and Pardue, M. T. (2010) Retinal function and structure in ant-deficient mice. *Invest. Ophthalmol. Vis. Sci.* **51**, 6744–6752
80. Berdoudo, E., Coleman, H., Lee, D. H., Stainier, D. Y. R., and Yelon, D. (2003) Mutation of weak atrium/atrial myosin heavy chain disrupts atrial function and influences ventricular morphogenesis in Zebrafish. *Development* **130**, 6121–6129